(12)

TRW

TRW Space & Technology Group

DSCS II Despin Pointing Anomaly

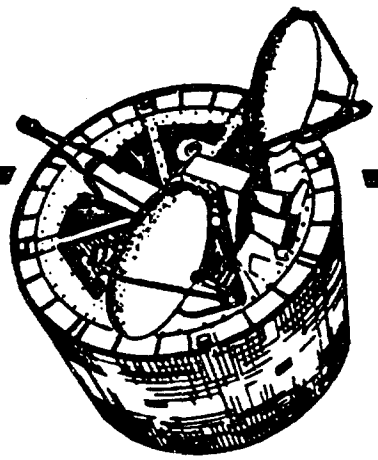

01 April 1983

Report No. 36060-AR-026
CDRL No. 009A6
F04701-80-C-0022

Approved for Public Release;
Distribution Unlimited

Prepared for

Space Division
Air Force Systems Command
Los Angeles Air Force Station
P.O. Box 92960, Worldway Postal Center
Los Angeles, California 90009

This report was submitted by the TRW, Defense and Space Systems Group, Redondo Beach, CA 90278 under Contract F04701-80-C-0022 with the Air Force Space Division, Deputy for Space Communications Systems, P.O. Box 92960, Worldway Postal Center, Los Angeles, CA 90009. It was reviewed and approved for TRW Defense and Space Systems Group by R. H. Alborn, Manager, DSCS II Orbital Operations. Lt Karen Gauthier, SD/YHD was the project engineer.

This report has been reviewed by the Office of Public Affairs (PAS) and is releasable to the National Technical Information Service (NTIS). At NTIS, it will be available to the general public, including foreign nations.

This technical report has been reviewed and is approved for publication. Publication of this report does not constitute Air force approval of the report's findings or conclusions. It is published only for the exchange and stimulation of ideas.

Karen A. Gauthier

KAREN A. GAUTHIER, Lt, USAF
Project Engineer

FOR THE COMMANDER

Gary W. Titmas

GARY W. TITMAS, Lt Col, USAF
Program Manager, DSCS Integration and Operations
Deputy for Space Communications Systems

REPORT DOCUMENTATION PAGE

READ INSTRUCTIONS BEFORE COMPLETING FORM

1. REPORT NUMBER: SD-TR-83-30	2. GOVT ACCESSION NO.: AD-A129815
3. RECIPIENT'S CATALOG NUMBER:	
4. TITLE (and Subtitle): DSCS II 9444 Despin Pointing Anomaly	5. TYPE OF REPORT & PERIOD COVERED: Final Report
	6. PERFORMING ORG. REPORT NUMBER: 36060-AR-026
7. AUTHOR(s): P. H. Fowler	8. CONTRACT OR GRANT NUMBER(s): F04701-80-C-0022
9. PERFORMING ORGANIZATION NAME AND ADDRESS: TRW Space and Technology Group, One Space Park, Redondo Beach, CA 90278	10. PROGRAM ELEMENT, PROJECT, TASK AREA & WORK UNIT NUMBERS:
11. CONTROLLING OFFICE NAME AND ADDRESS: Space Division, Department of the Air Force, P.O. Box 92960, Los Angeles, CA 90009	12. REPORT DATE: 01 April 1983 13. NUMBER OF PAGES: 84
14. MONITORING AGENCY NAME & ADDRESS (if different from Controlling Office):	15. SECURITY CLASS. (of this report): Unclassified 15a. DECLASSIFICATION/DOWNGRADING SCHEDULE:

16. DISTRIBUTION STATEMENT (of this Report)

Approved for Public Release; Distribution Unlimited

17. DISTRIBUTION STATEMENT (of the abstract entered in Block 20, if different from Report)

18. SUPPLEMENTARY NOTES

19. KEY WORDS (Continue on reverse side if necessary and identify by block number)

Despin bearings, DSCS II Satellites

20. ABSTRACT (Continue on reverse side if necessary and identify by block number)

Presents the results of an investigation of minor intermittent pointing wander in 9444 and other DSCS II satellites. Ascribes the effect to sticking in the preload mechanism, and shows numerical reasons for this conclusion.

DSCS II DESPIN POINTING ANOMALY

Report No. 36060-AR-026
CDRL No. 009A6
F04701-80-C-0022
01 April 1983

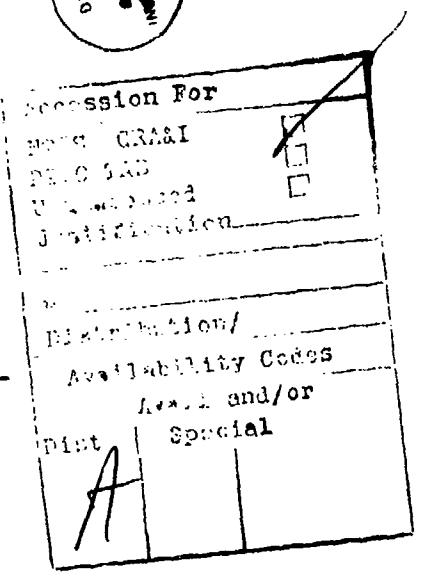

Prepared by: _____
P. H. Fowler

Approved: _____
H. B. Benner, Jr.
Manager
DSCS II Project

Approved: _____
R. H. Alborn
Manager
DSCS II Orbital Operations

TRW

TABLE OF CONTENTS

1. INTRODUCTION

The Defense Satellite Communications System Phase II (DSCS II) satellite consists of a spinning section, carrying power and TT&C systems, supporting a despun section containing the communication payload. The despun section is pointed at the earth, using earth sensors on the spinning section as a reference. The spinning section weighs in the vicinity of 1,000 lbs., and the despun section about 400 lbs. The two sections are joined by the "Despin Mechanical Assembly" (DMA) consisting of dual motors, resolvers, and power and signal sliprings. The structural bearings are a pair of angular contact 1/2" ball bearing sets of slightly different diameter. The top inner race is free to move on the shaft, and is preloaded by a ring of spring loaded plungers acting through a thrust washer. The spinning section turns at about 1 RPS, the exact speed depending on the propulsion and expendable (hence moment of inertia) history of the individual spacecraft. Figure 1 shows the general appearance of the DMA.

Almost from launch, DSCS II satellite 9444 has had periods of pointing disturbance. Typically, pointing wander of 1/2° would develop over a period of a few minutes, followed by an abrupt return to normal quiet behavior (< 0.1°). The effect seems to be partly seasonal, and long periods have elapsed without any events being noted. (Since the satellite is usually monitored only for one 15 minute period per day it is not certain that observed quiet periods are truly indicative of event-free performance 24 hours per day.) Typically, the platform running torque steady state is different from before to after an incident (as shown by telemetry).

2. ORBITAL DATA

Table 1 shows a history of known pointing peculiarities. Figures 2, 3 and 4 show typical pointing events.

The events of Figures 2 and 3, among others, were subject to Fourier analysis by Aerospace Corporation, with results shown

Figure 1

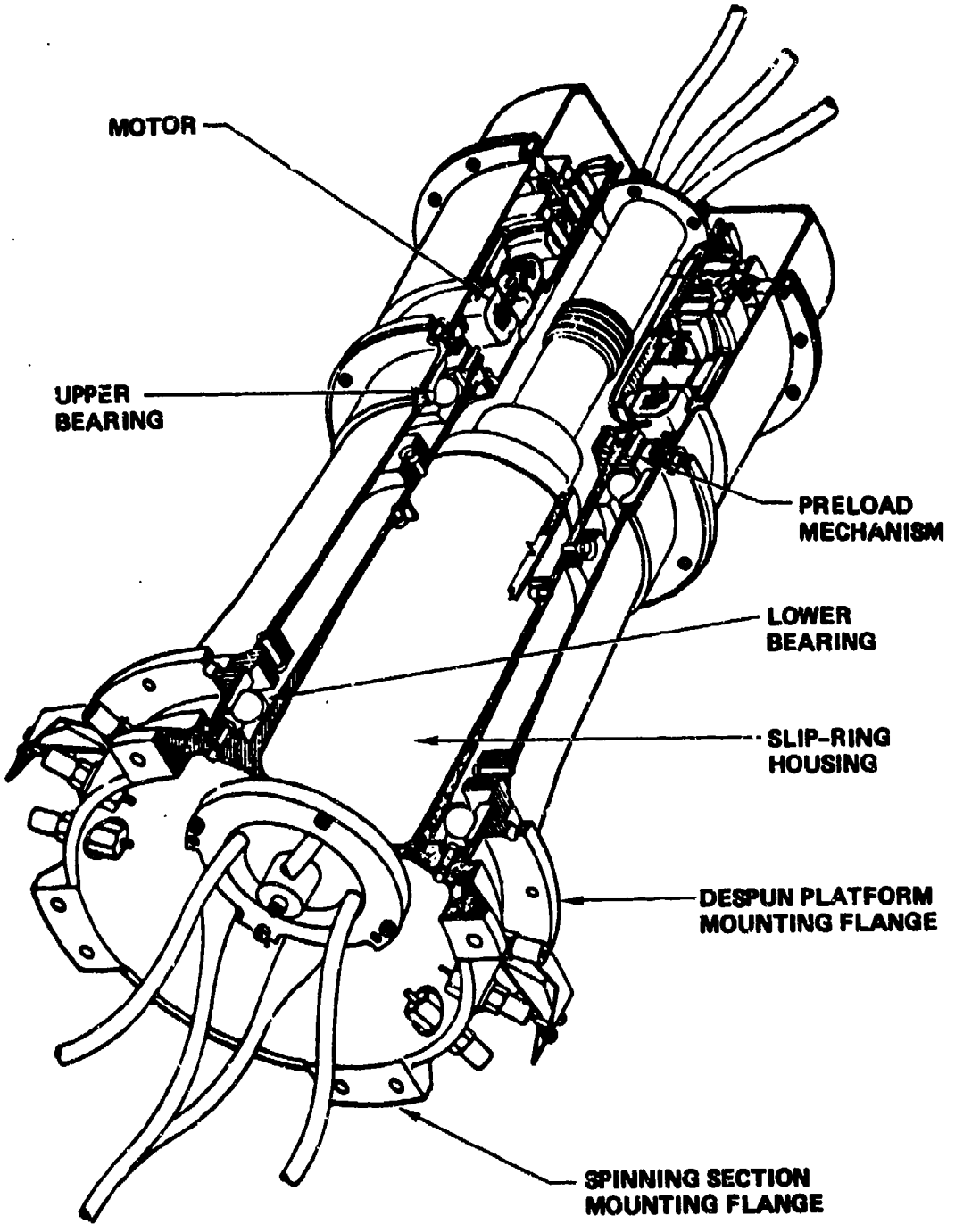

DMA CUTAWAY VIEW

Table 1

9444 DESPIN POINTING CHRONOLOGY

Date	Time (Z)	Event
11/21/79	0210	Launch
	1134	Despin in Rate Mode (CTA-1, DEA-1, ESAs-1)
11/23/79	2113	Normal Mode, GS-7
11/24-11/27/79		Gain State Evaluation (GS-6, 5, 4, 5)
12/7/79		Transients of +.2, -.3° Started Occurring
12/11/79	0330	GS → 7
12/13/79		CTA-1 → -2, DEA-1 → -2
1/17/80		Transients Ceased
11/22/80-3/2/81		Storage (Rate Mode)
1/31/81	0500	GS → 5
4/28/81		+.1, -.3° Transient
5/14/81		±.6° Transient
5/15/81	0500	GS → 7
5/26/81, 6/1/81		+.2, -.3° Transients
7/5, 7/6/81		±.4° Transients
7/18/81		±.3° Transients
8/21/81		±.3° Transients
8/24, 8/25/81, 8/26/81		±.4° Transients
10/29/81		+.2°, -.5° Transients
11/3/81		±.4° Transients
11/5/81		-.4° Transient
11/7/81		+.2, -.4° Transient
11/12/81		+.2, -.4° Transient
1/1/82		-.3° Transient
1/14/82		+.3, -.4° Transient
7/21, 7/22/82		+.2, -.3° Transients
7/23		-.4° Transient

Figure 2

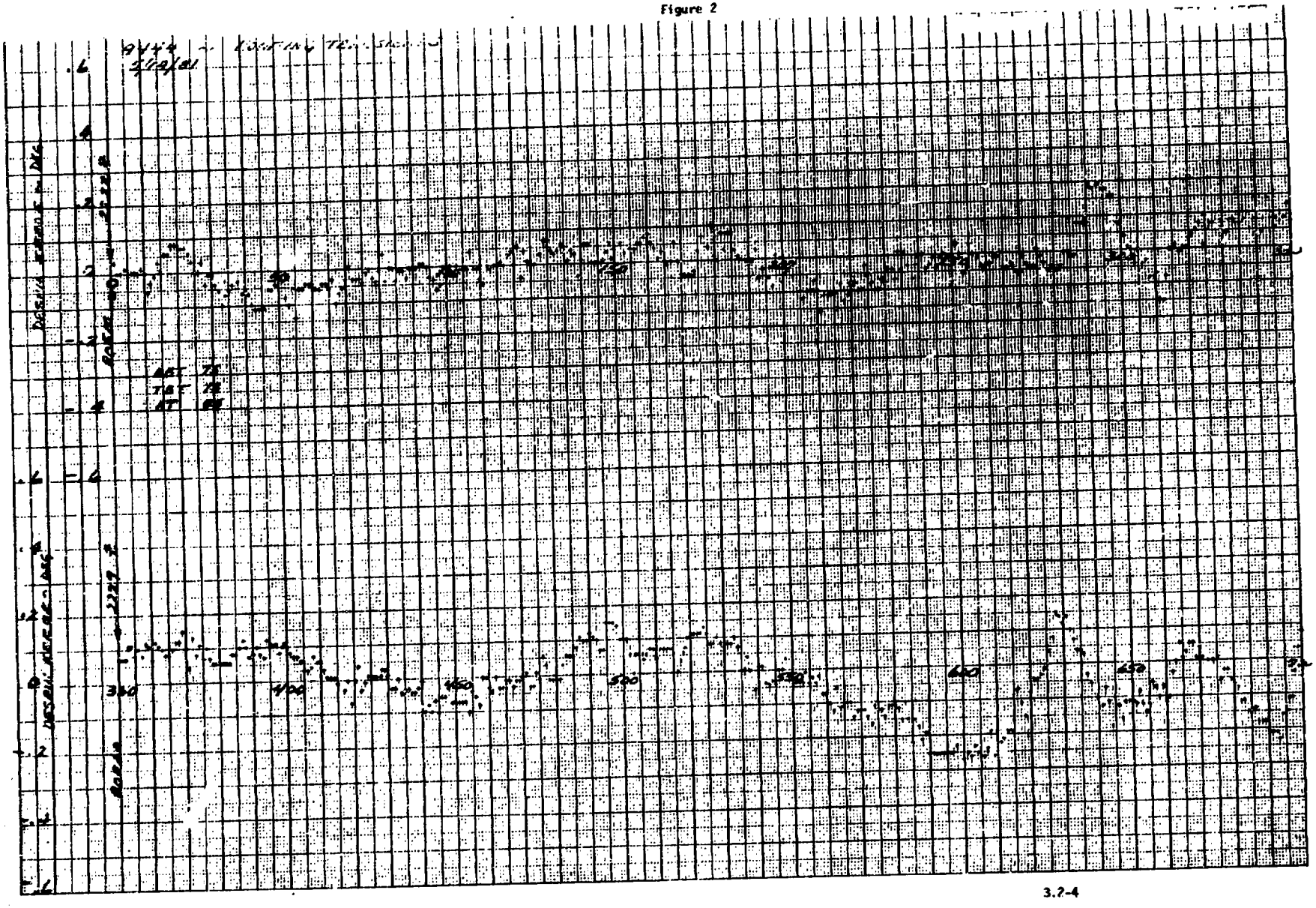

Figure 2 (Cont'd)

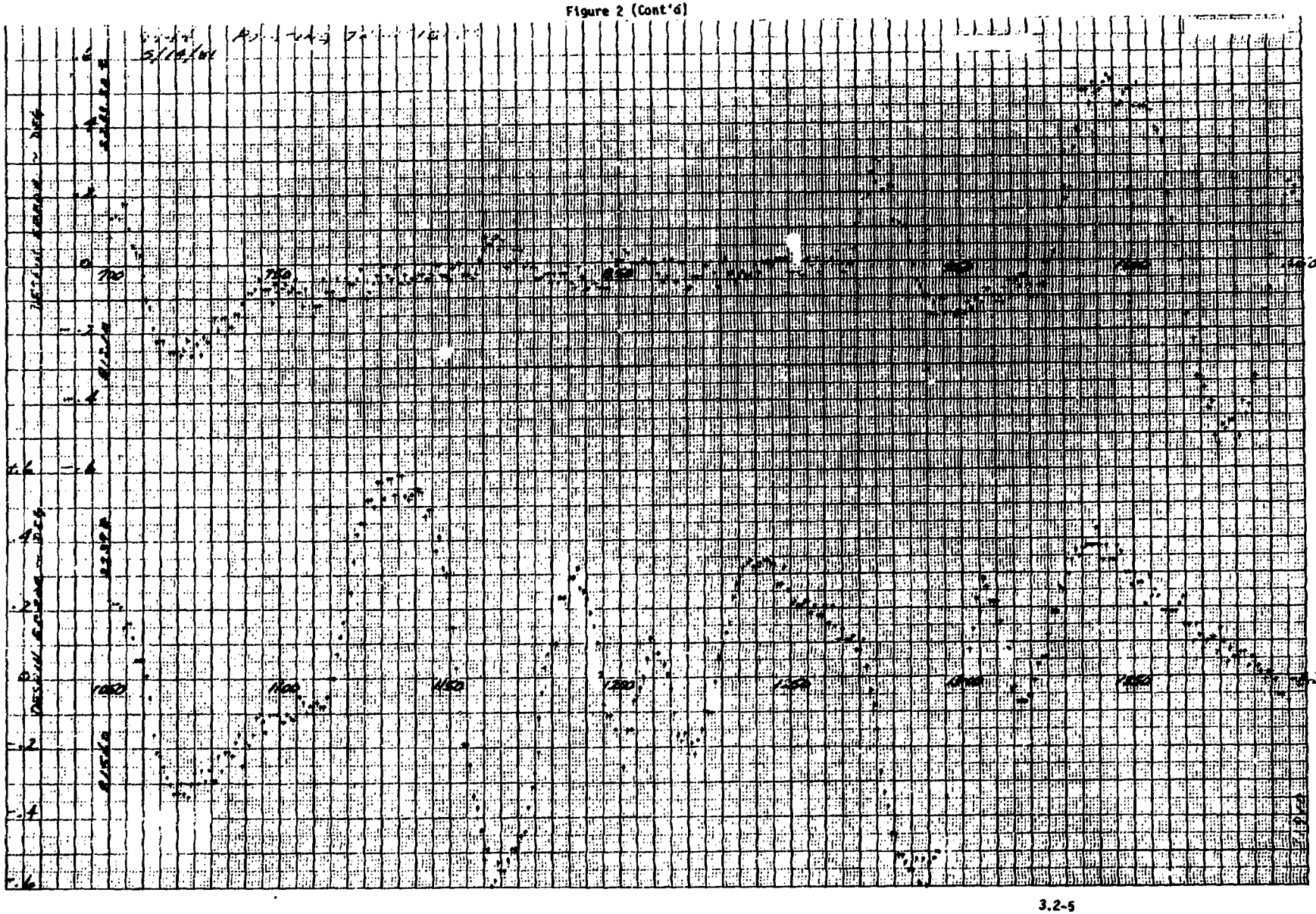

Figure 2 (Cont'd)

Figure 3

9444 28 MARCH 1981

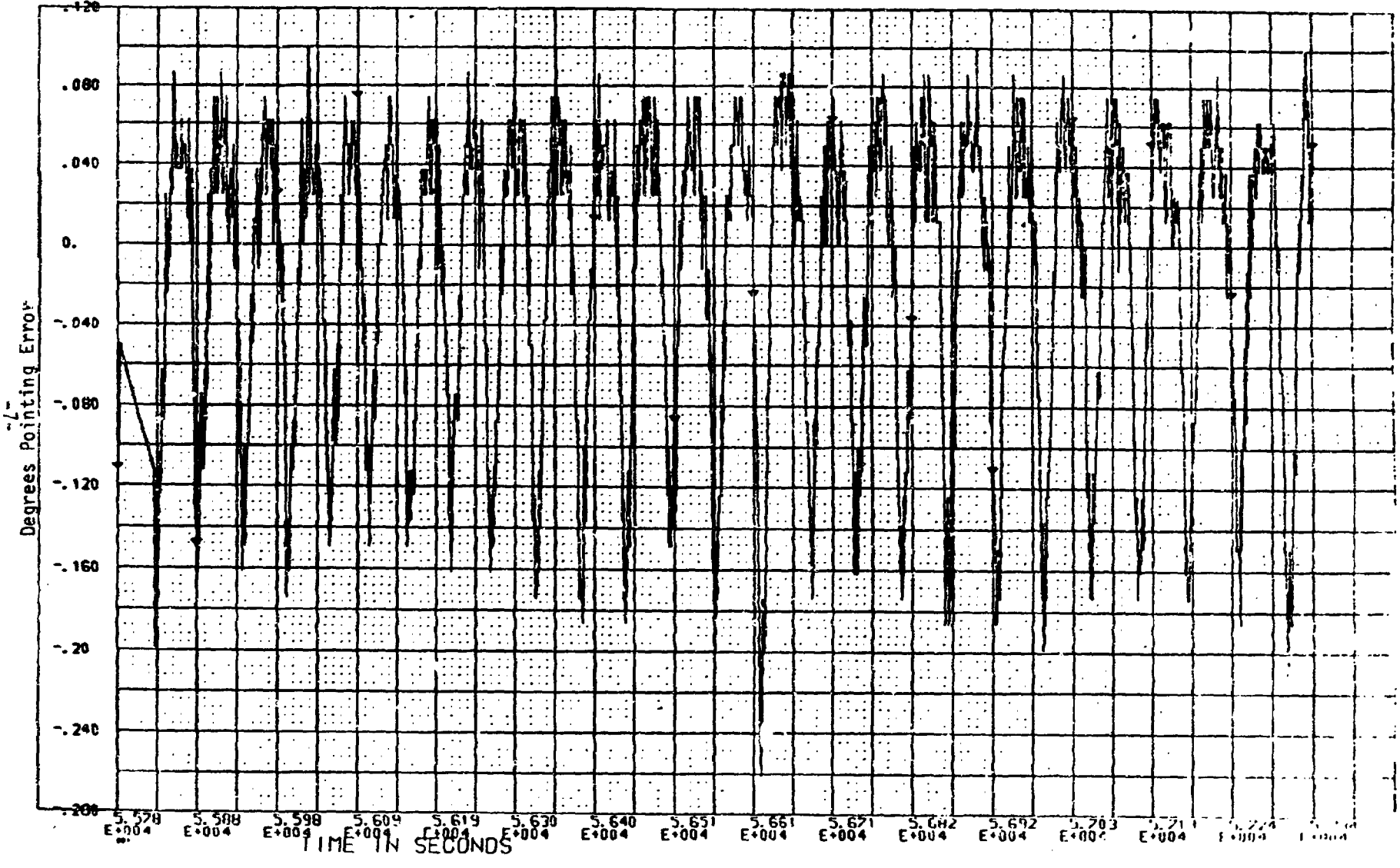

Figure 4

9444

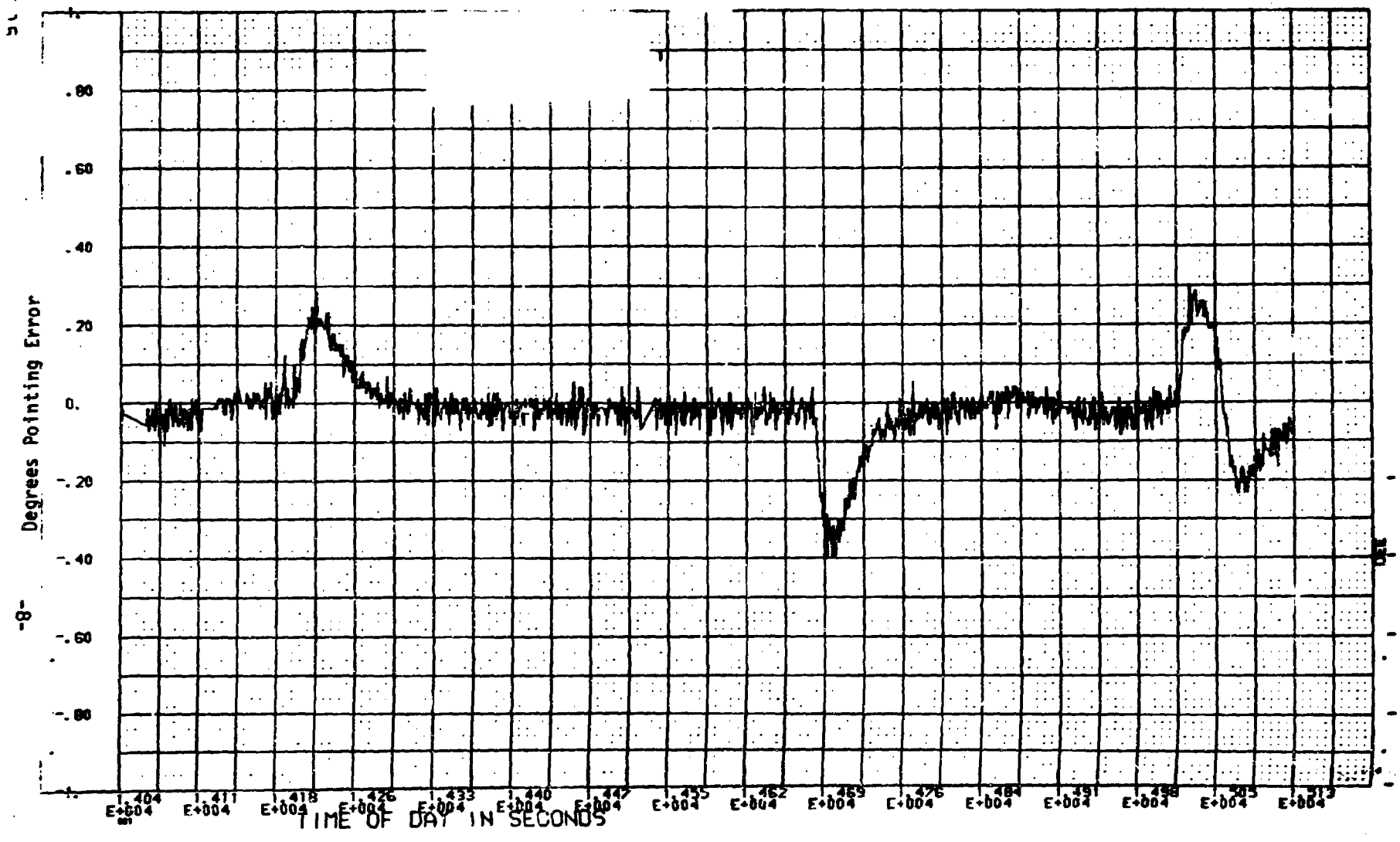

in Figures 5 and 6. Figure 7 shows the autocorrelation of Figure 2. Note that the analysis shows the events to consist of a mixture of sine waves, and that they are not of the nature of a random back and forward motion. Figure 8 shows the TORQ* signal of the event in Figure 4.

3. CANDIDATE CAUSES

It is evident from the telemetry records that a real disturbance to the torque needed to maintain pointing is taking place. This is indicated by the spacecraft maintaining good earth pointing (not loosing lock) with long term steps in the TORQ signal, since if these were the result of an electrical malfunction an unbounded pointing error would develop.

Torque irregularities may originate within the DMA, or could be caused by inteference between the despun platform and the spinning section. However, interference would produce a torque spike at one cycle/rev., which would not produce the observed pointing effects. In all likelihood, a once/rev. disturbance would be observed only as a steady torque, and would produce no obvious pointing effect.

Computer simulation (see Appendix I) demonstrates that the control system is well damped, and that sinusoidal motions are produced only by sinusoidal torques. The observed oscillatory incidents are thus not the system response to torque transients, though Figure 4 shows that some events are of the nature of single torque steps. In no case is the signature the result of torque noise - it is either driven by torque steps or by a clearly defined mix of sinusoidal torques at very low frequencies. The simulation also shows that the driving torque causing the disturbances is typically 1 to 5 in.-oz.

---

*"TORQ" is the telemetry indication equivalent to drive applied to the DMA motor.

Figure 5

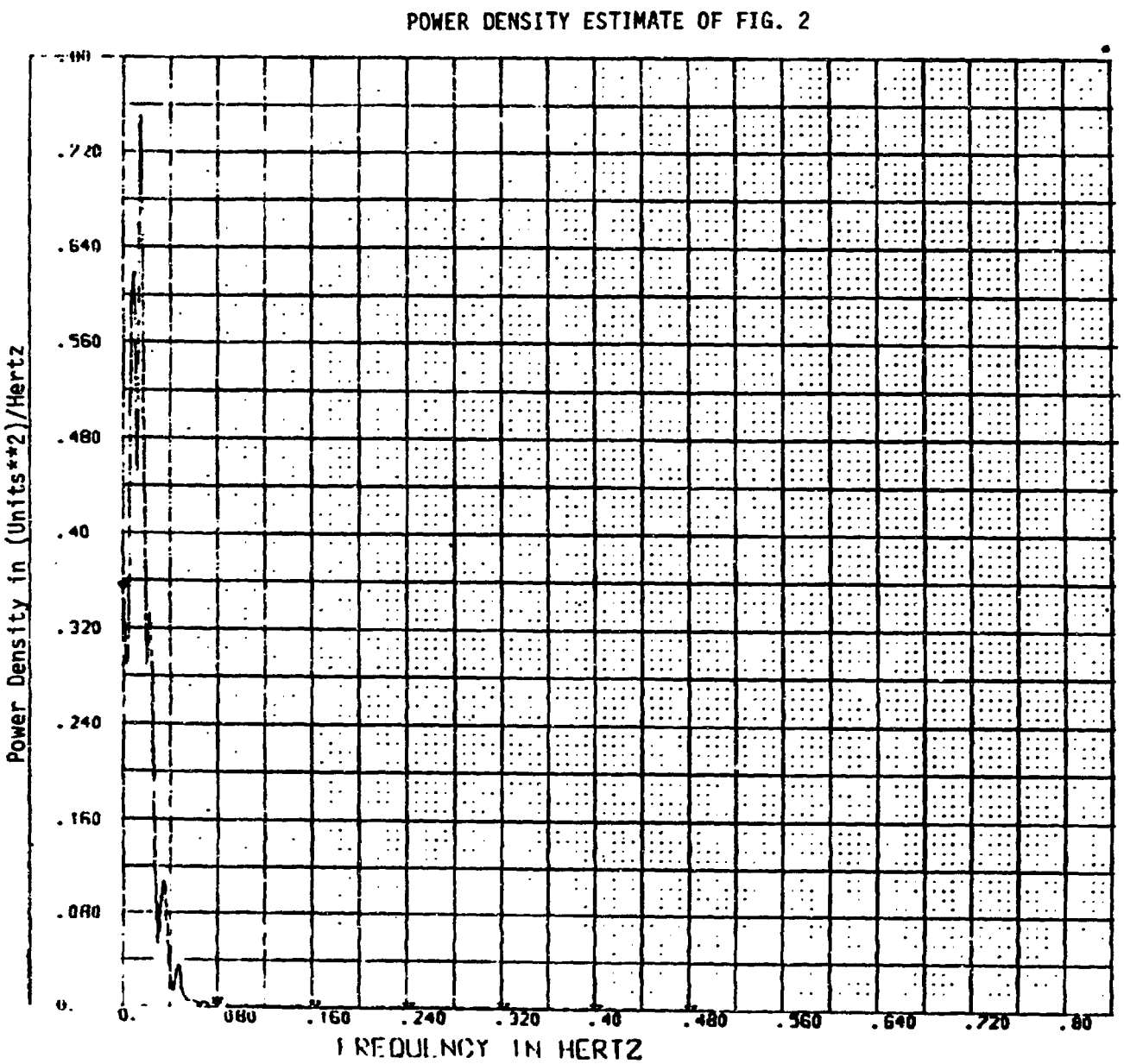
POWER DENSITY ESTIMATE OF FIG. 2
Power Density in (Units**2)/Hertz
.720
.640
.560
.480
.40
.320
.240
.160
.080
0.
0.
.080
.160
.240
.320
.40
.480
.560
.640
.720
.80
FREQUENCY IN HERTZ

Figure 6

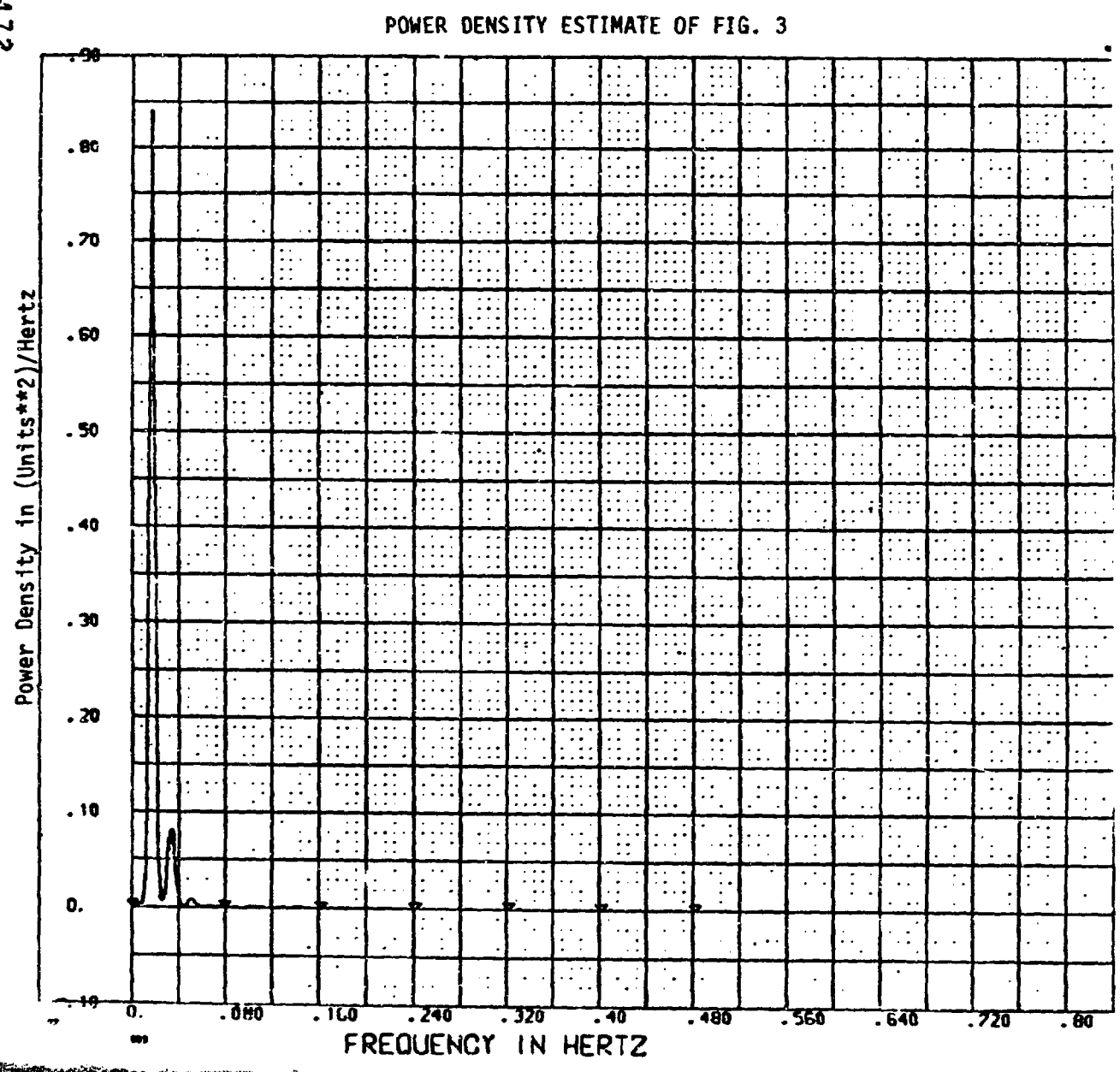
POWER DENSITY ESTIMATE OF FIG. 3
Power Density in (Units**2)/Hertz
.90
.80
.70
.60
.50
.40
.30
.20
.10
0.
0.
.080
.160
.240
.320
.40
.480
.560
.640
.720
.80
FREQUENCY IN HERTZ

Figure 7

AUTOCORRELATION ESTIMATE OF FIG. 2

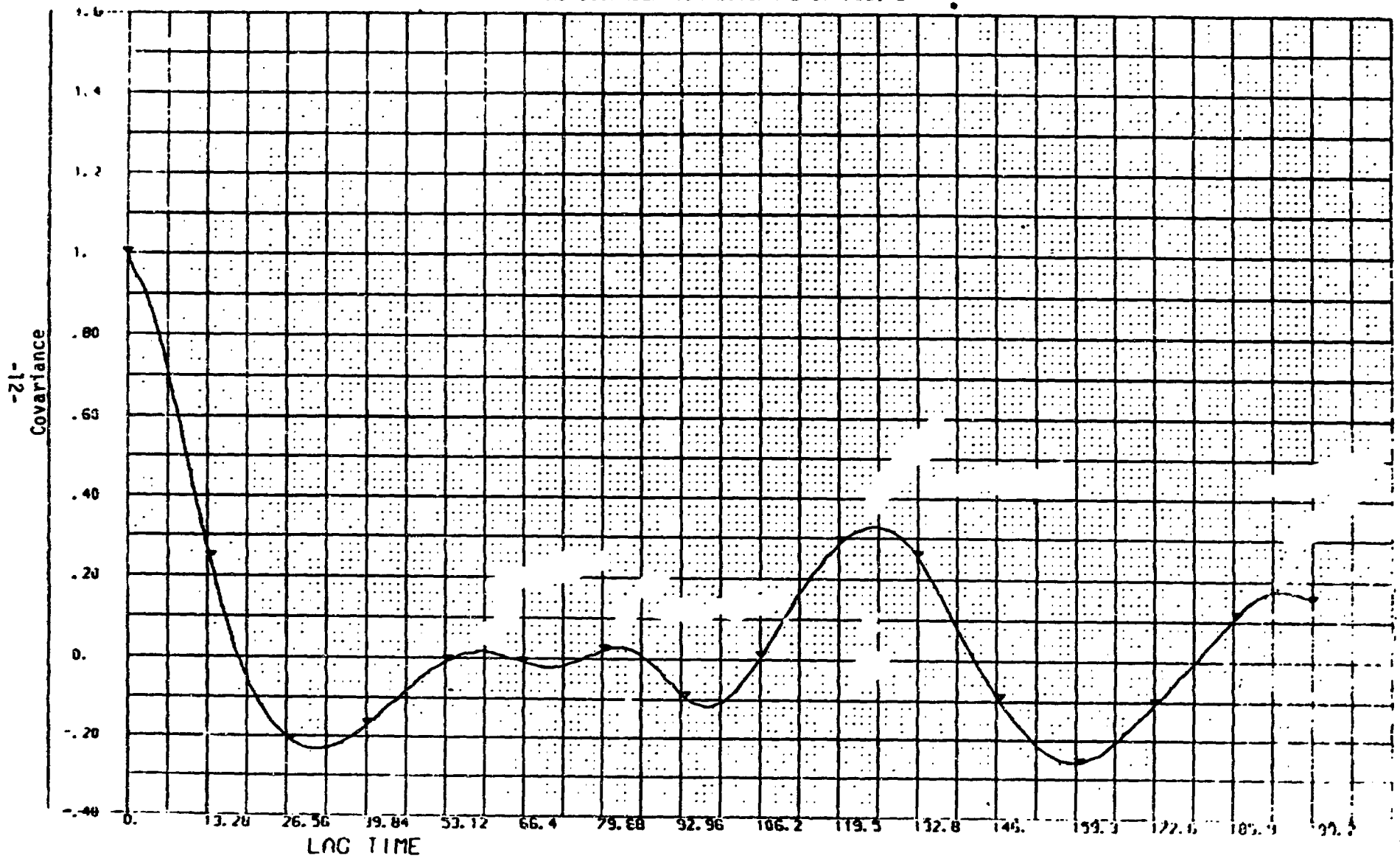

Figure 8

9444

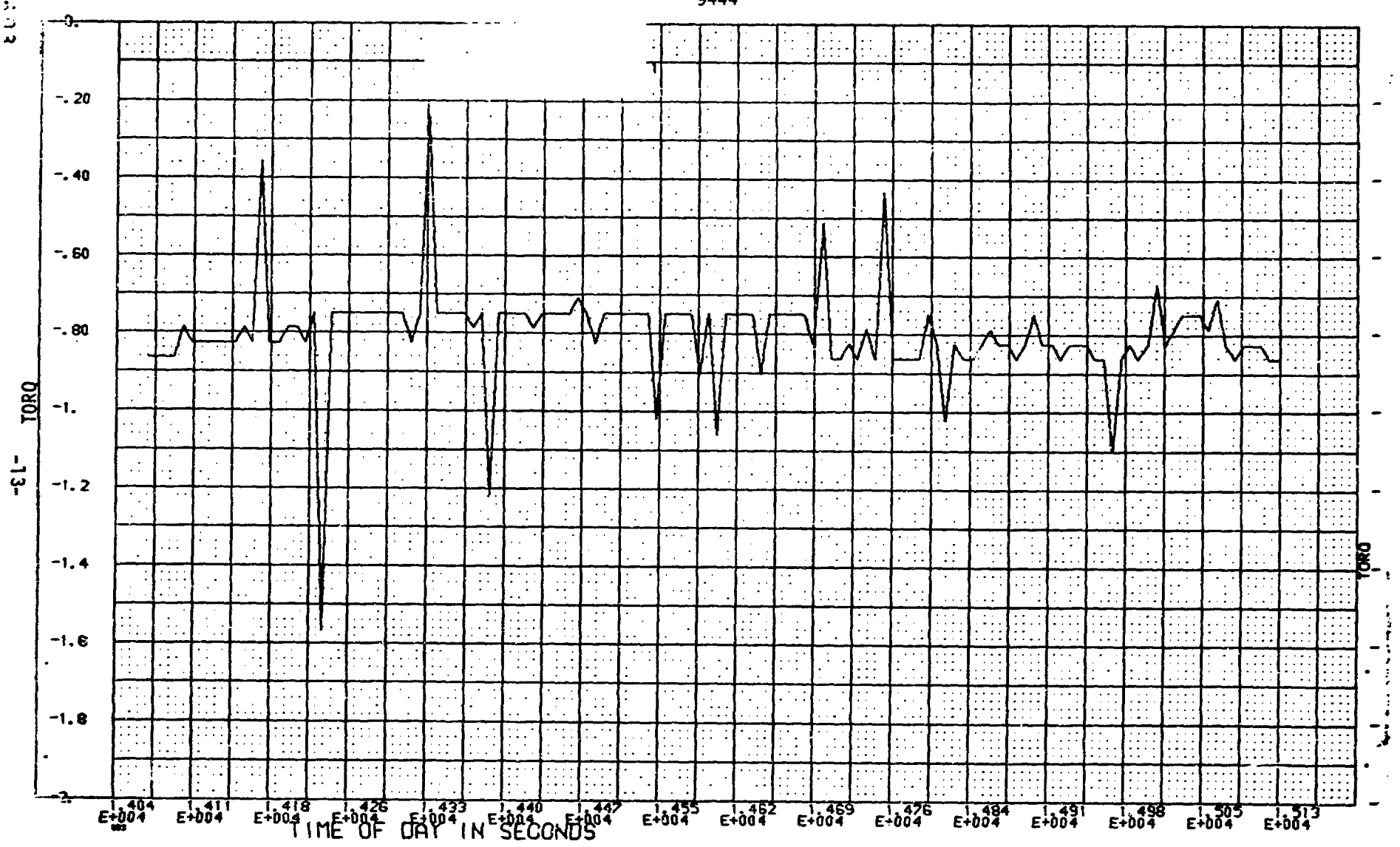

The major DMA functional components are the motor/resolver stack; the slipring and bearing assembly; the shaft, preload, and main bearing assembly; and the housing. The analysis following attempts to explain the anomaly in terms of interaction of these components.

DSCS II satellites 9433 and 9434 have histories of similar appearing behavior, culminating in the loss of 9433 ascribed to jamming of the top bearing. 9434 has operated for nine years, and has episodes of pointing wander containing similar sinusoidal components to 9444. Neither 9434 nor 9444 show any signs of degrading performance. It is therefore evident that an explanation of the DSCS II pointing anomalies must assume they may be within the normal range of behavior of the assembly, though with sporadic occurrence both in time and across the population.

4. EXAMINATION OF FREQUENCY COMPONENTS

The most puzzling aspect of the orbital signature is the existence of very long period sinusoidal components representing appreciable torques. The obvious periods associated with the DMA are short and mostly above the frequency which would produce any observable effect on the platform pointing. The fundamental rotation speed is near 1 Hz, and the balls generate a noticeable signal about 10 Hz. The retainer speeds are about .5 Hz.

A study by Ball Aerospace Division, Appendix 2, shows that there are subtle low frequency components in the motions of the ball train. However, these motions would account for frequencies which were continuously present in all DMAs, and would not obviously result in intermittent spells of pointing wander.

The shaft axis direction relative to the housing is determined, on a microscopic scale, by the position of the various size balls in the top and bottom bearings relative to the minor geometric

irregularities of the races. Since the ball train speeds are slightly different, the shaft describes a very small complicated coning motion at speeds which are beats between the two bearing retainer speeds. The actual frequencies produced are a function of the geometry of the races and balls, and the instantaneous contact angles of the bearings. A set of representative cases has been analyzed (Appendix 3), showing a tendency for the resulting shaft motion to have frequency components similar to those seen in the orbital data. However, while the motion would change in amplitude and frequency with time and temperature, it would not in itself produce periods of abnormal wander, and certainly would not show abrupt returns to quiet pointing.

Thus, it appears that the main bearings individually and as an assembly produce low frequency motions of the shaft similar to the orbital signature. However, the cause of the amplitude envelope of the orbital disturbances must be looked for elsewhere.

5. POSSIBLE DISTURBANCES TO BEARING MOTION

It appears essential to the transient nature of the pointing disturbance that something changes position within the DMA in such a way as to disturb the ball train motions. There are only two elements in the unit capable of irregular motion: The bearing retainers and the preload mechanism.

The retainers are capable of producing the torque signature of Figure 4 by touching one of the lands. However, there does not seem to be a retainer motion which would cause a slowly rising disturbance as seen in Figure 2 — the retainer is turning too fast to have stable unidirectional radial or axial motions extending over several minutes. Bearing effects of retainer motions are reported as high frequency "squeals" or short erratic torque noises, not as long regular events taking hundreds of revolutions to complete.

The preload mechanism, Figure 9, by design, is capable of several motions. The pistons move in and out to accommodate temperature induced motions in the assembly, the thrust washer and pistons can rotate through a small angle, and the top bearing inner race can move up to $\pm$ .0005 in. radially on the shaft.

There is the equivalent of a rotating load turning with the shaft due to the small residual out-of-balance of the spinning section. This amounts to an equivalent shaft out-of-line with the c.g. of .08°. The above mentioned inner race clearance amounts to a potential .008° change in shaft direction, or 10 percent of the normal out of balance.

Over the range of differential temperatures of the shaft and housing, the motion of the preload pistons is of the order .0005 in. Since there is no torque stay in the mechanism, the few ounce drag of the top bearing tends to tilt the preload pistons slightly and push some of them to the edge of their holes. The pistons and the holes are not finished to bearing standards, and are capable of sticking when side loaded. (Experiments with a spare unit show some pistons can easily be made to stick by tilting.)

Should a piston stick, the inner race can be tilted of the order .0005 in., which is around the maximum that the shaft clearance will allow. As mentioned above, this has the effect of disturbing the ball motion and of adding up to 10 percent to the spacecraft apparent out of balance.

While the numerical effect of this is difficult to predict, it should be noted that a bearing run with a 1 mil tilt deliberately introduced and washed free of lubricant locked up solid in a few hours running. It was found however, that the bearing would not lock up under this condition if amply lubricated. The running torque unlubricated, until the

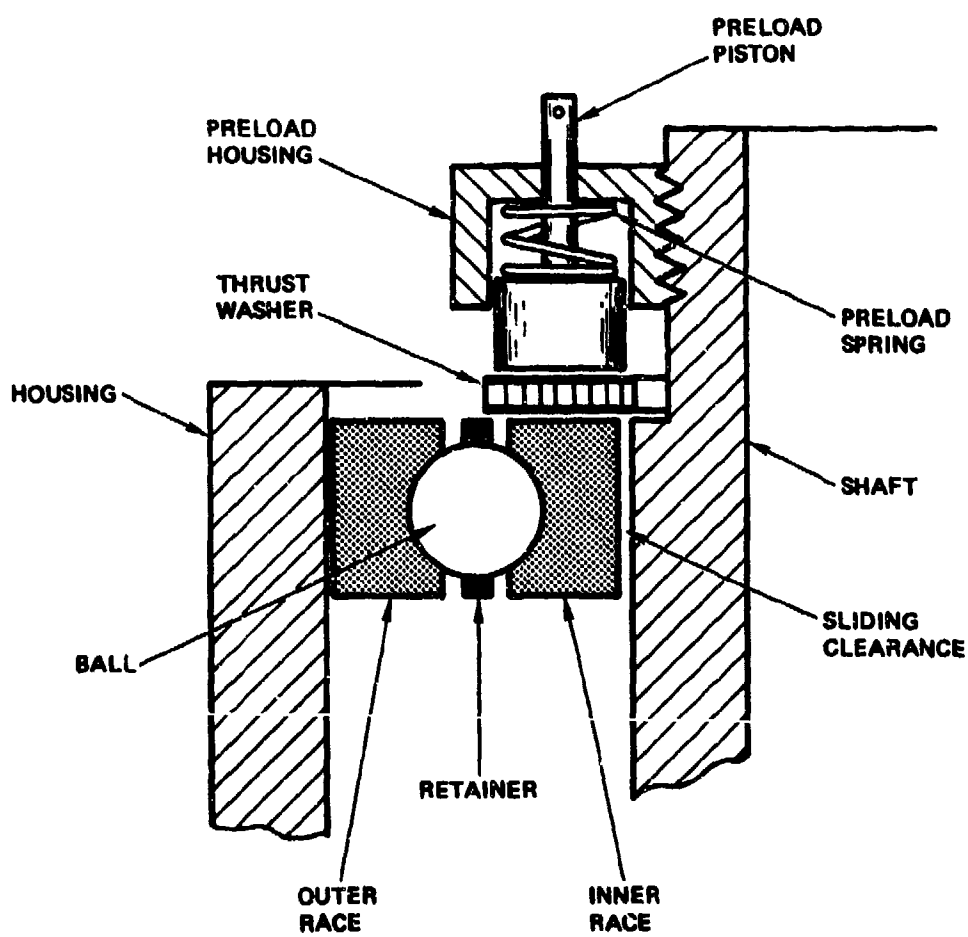

Figure 9A. Preload Schematic Section

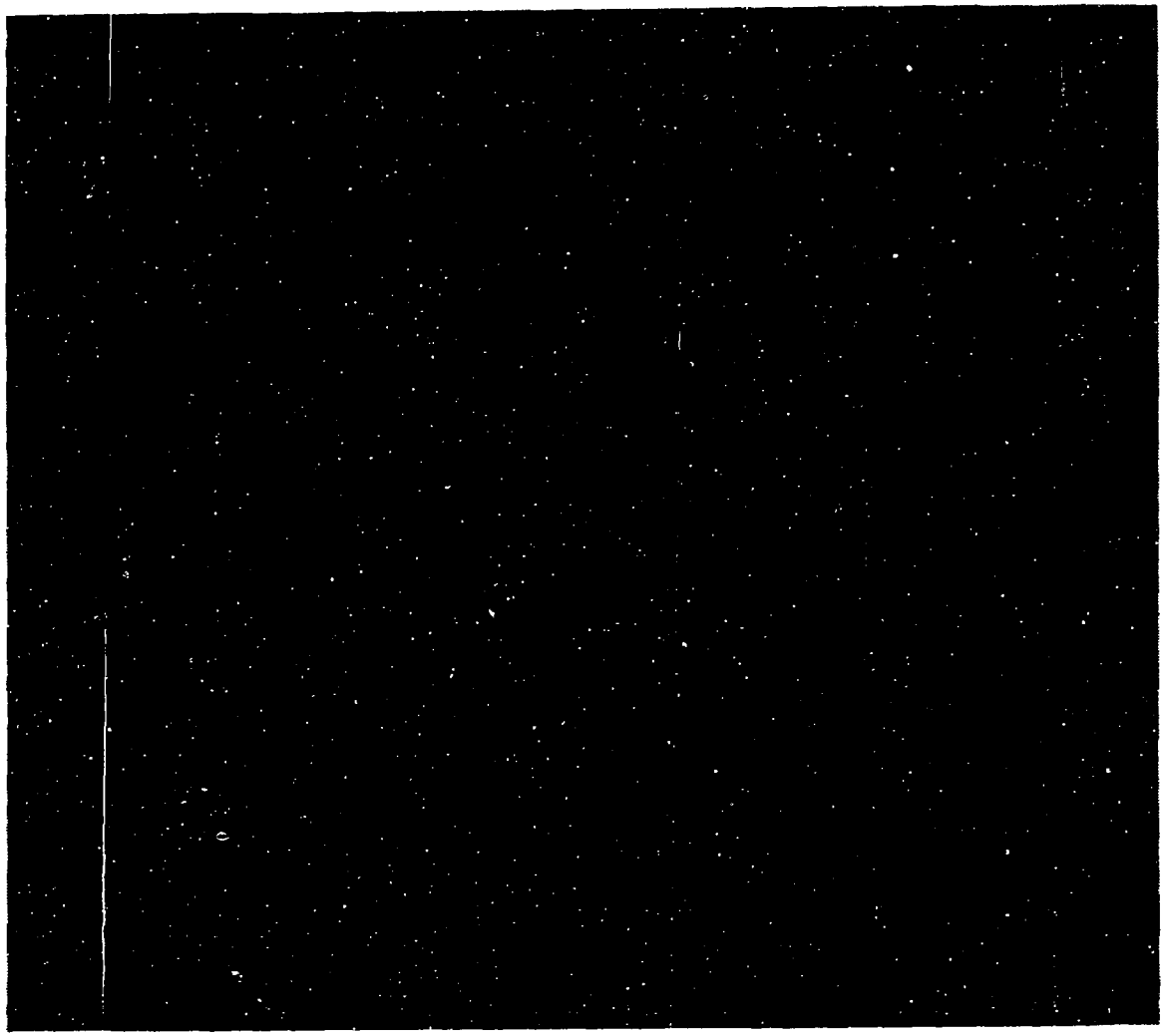

Figure 9B. Preload Assembly

Figure 9C. Preload Piston Faces

point of failure approached, was about 20 in.-oz. It can certainly be expected that severe torque disturbances will result from maintaining a tilt in the inner race.

Note that at the preload of 60 lbs. and with 21 and 23 balls in the races, the average preload per ball is just under three lbs. At a well lubricated limiting coefficient of friction of about 0.1, the force at which a ball will slip is thus about .3 lbs. This force acts on a 2 in. radius, or a torque of just under 10 in.-oz. This happens to be the torque equivalent of .6° of wander (see Appendix I). It can thus be speculated that the structure of torque ramps and steps inside various pointing events is produced by the balls pinching the retainer up to the maximum force they can react on the race. It can also be seen that so long as there is ample lubrication the balls cannot exert significant forces on the retainer, and cannot generate significant amounts of heat (10 in.-oz. $\sim$ .1 cal/sec). The event occurrence is thus speculated to be due to the preload pistons sticking and tilting the inner race, triggering ball riding on the retainer and stick-slip behavior producing the observed torque.

6. CONCLUSIONS

Sections 4 and 5 have presented reason to believe that the frequency content and amplitude of the orbital disturbances are explicable as due to disturbances caused by intermittent sticking of the preload mechanism. Since it is impractical to duplicate the orbital DMA operation in ground test, the mechanism of pointing wander cannot be known with certainty.

However, it has been proposed by several observers that sticking of the preload mechanism is the most likely cause (e.g., letter from COMSAT Corp. to Aerospace Corp. of January 14, 1976 Re: 9433 Failure). Several design improvements would preclude this type of problem, for example:

- The preload pistons could be a bearing quality fit and finish in the housing.

- The preload could be applied by a "wavy washer" or similar device incapable of sticking.

- Modern mechanisms of this type use a diaphragm spring moving support also incapable of sticking.

Both experiment and experience with later well-lubricated DMA bearings suggest that the condition will only lead to failure in an unlubricated system. The corrective actions taken after the 9433 failure included increased lubrication and reduced volatiles in the retainer. Both those improvements reduce the chances of a tilted bearing locking up due to evolution of material from the retainer jamming the balls.

Appendix I

CALCULATED CONTROL SYSTEM RESPONSES

TRW
DEFENSE AND SPACE SYSTEMS GROUP
ONE SPACE PARK • REDONDO BEACH • CALIFORNIA 90278

INTEROFFICE CORRESPONDENCE

82.L033.11-007

TO: A. H. Rosenberg

CC: R. H. Alborn
H. B. Benner
R. A. Cash
R. E. Edwards
P. H. Fowler
I. J. Williams

DATE: 1 March 1982

FROM: R. E. Greenwood

BLDG 82 MAIL STA. 2766 EXT. 50751

SUBJECT: DSCS II Disturbance Frequency Response by Simulation

Recently there has been some discussion on the frequency response of the DSCS II control system to sinusoidal disturbances. There have been numerous parameter changes in the system since 1969 when T. Bierma did his analysis. I have reproduced page 219 of his report 69.7231.9-70 (777-F2-282) as Figure 1. In this IOC the parameters of the 9444 satelite are used in the DSCS II Simulation to compute the frequency response to a sinusoidal torque disturbance. The result is shown in Figure 2. Note that the 9444 satelite is less than 30% as sensitive to sinusoidal torques as the DSCS II system originally was designed. The peak frequency is somewhat less also.

This IOC also shows a series of step and pulse simulations. Most of the torques used here have an amplitude of 10 in-oz, which was taken as a matter of convenience. Figures 3 to 11 shown the uncompensated pointing error accompanying the torque disturbance for a step change and for various pulse widths. Figures 12 to 14 show the compensated pointing error waveforms for the cases of a step in torque and brief pulses of torque. It should be noted that the simulation responses of Figures 8 to 10 are nearly identical. Presumably this is because the pulses are so fast as to act like impulses and, hence, only the area of the pulse matters. A comparison of Figures 8 and 11 shows that a change in polarity of a friction torque results in a pointing transient of opposite polarity.

As the available 9444 data do show some characteristics such as seen in Figures 3 to 11, and especially Figures 8 to 10, it is possible that the step-like behaviour of 9444 could be explained by a series of rapid engaging and disengaging friction sources. Amplitudes of up to $\pm$ 10 in-oz for these frictions are consistent with the 9444 data.

REG:lr

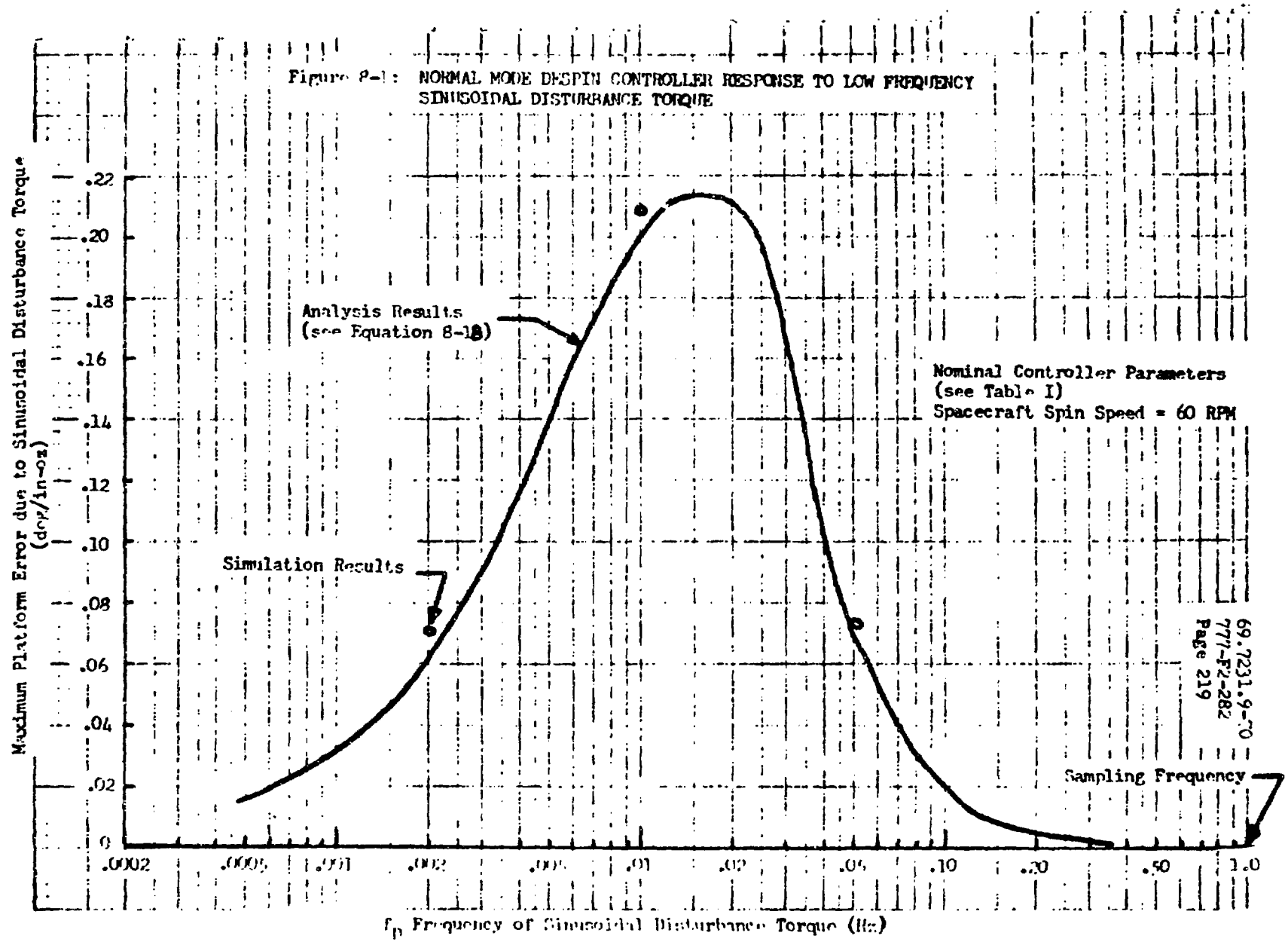

Figure 1. Original DSCS II Response to Sinusoidal Torque Disturbances.
Reproduced from Bierma report 69.7231.9-70 (777-F2-282)

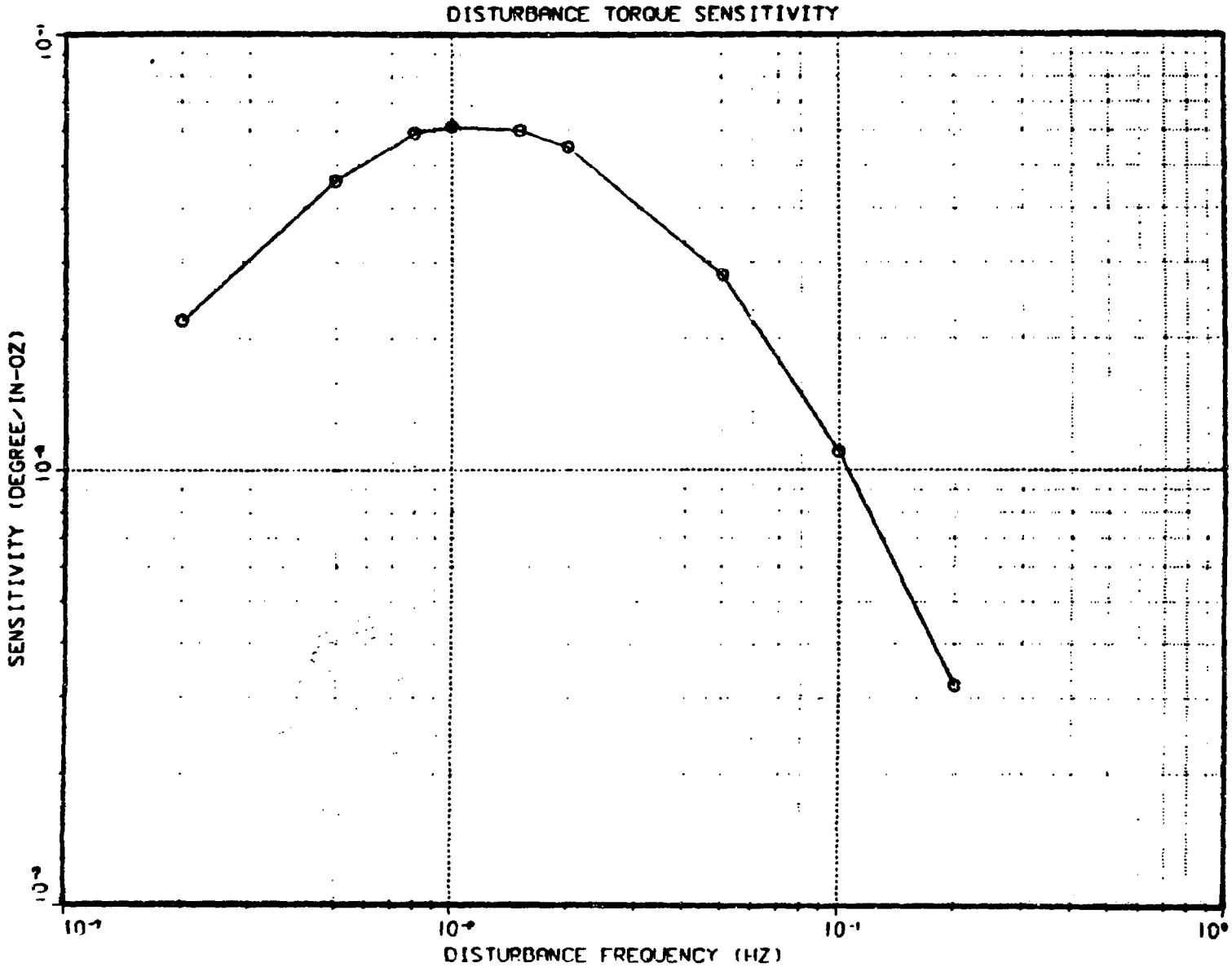

Figure 2. Current 9444 Response to Sinusoidal Torque Disturbance.

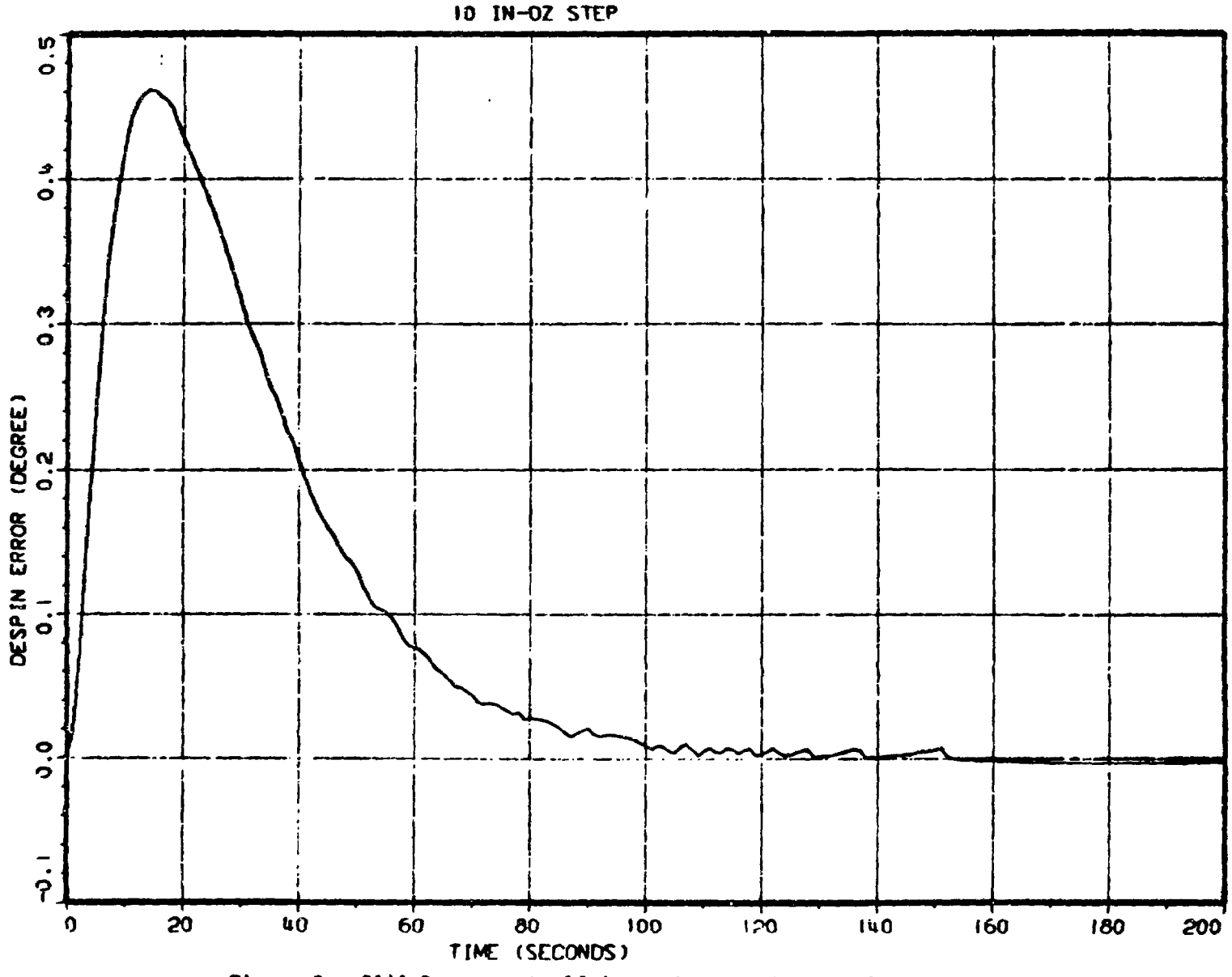

Figure 3. 9444 Response to 10 in-oz Step of Torque Disturbance.

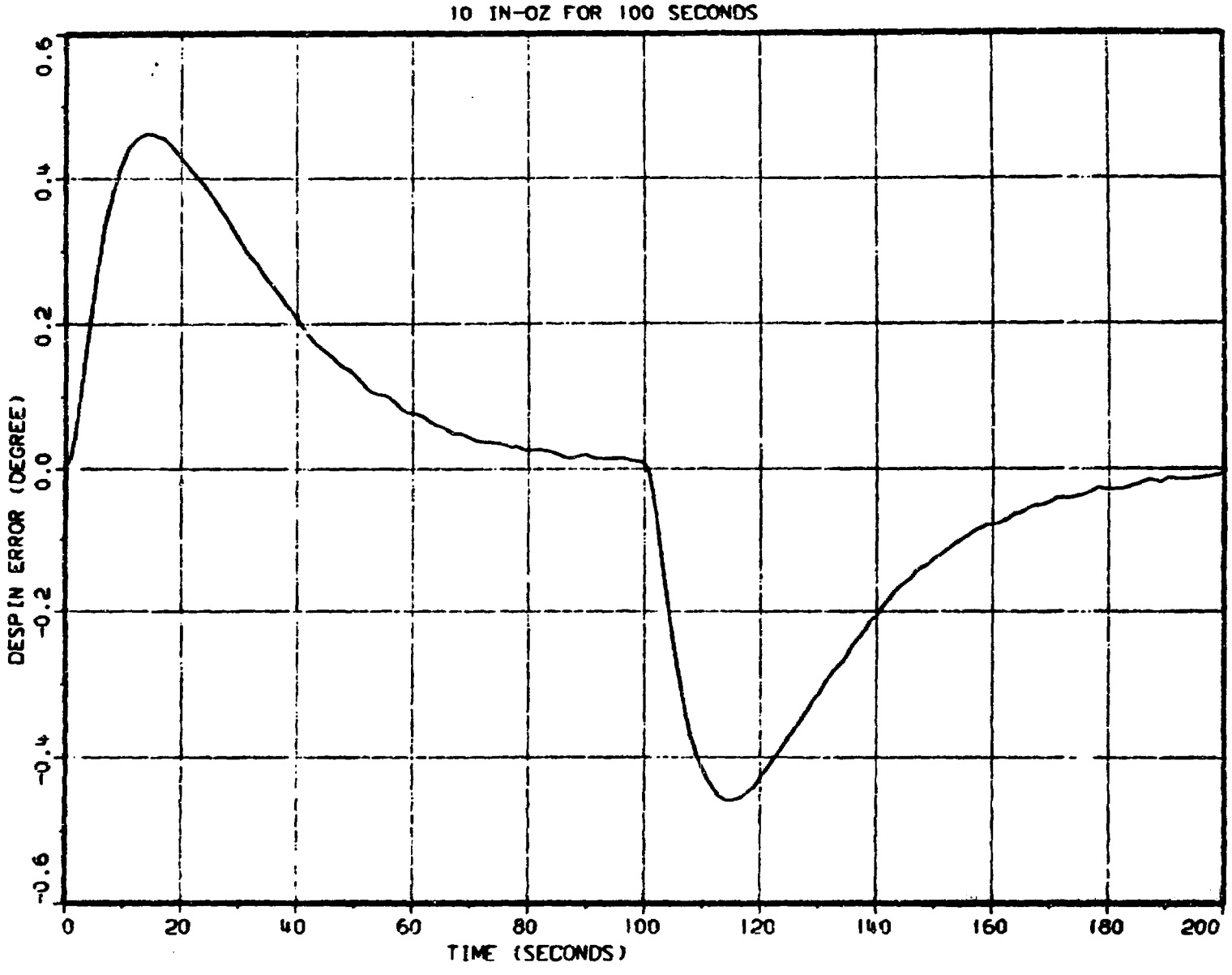

Figure 4. 9444 Response to 10 in-oz 100-second Pulse of Torque Disturbance

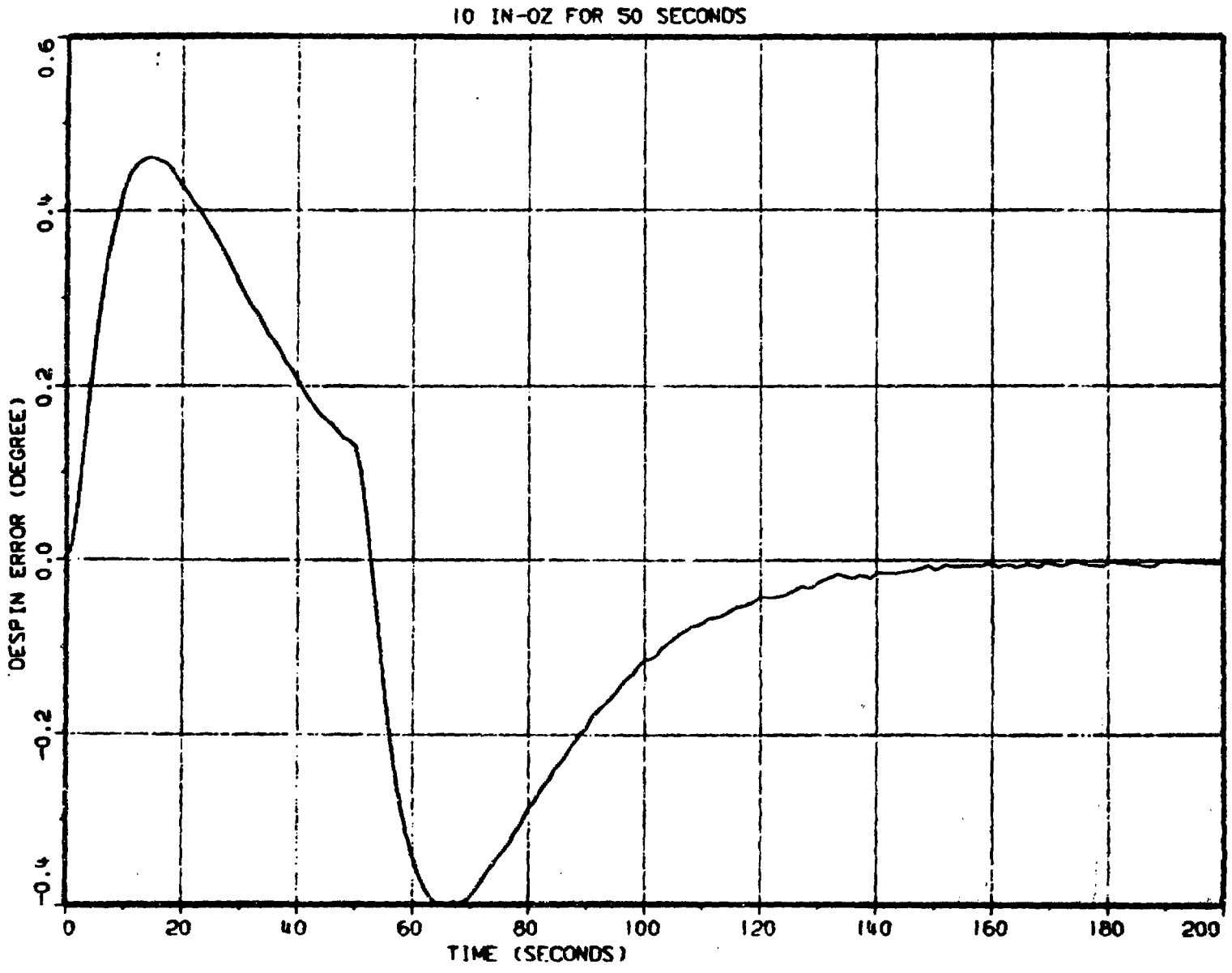

Figure 5. 9444 Response to 10 in-oz 50-second Pulse of Torque Disturbance

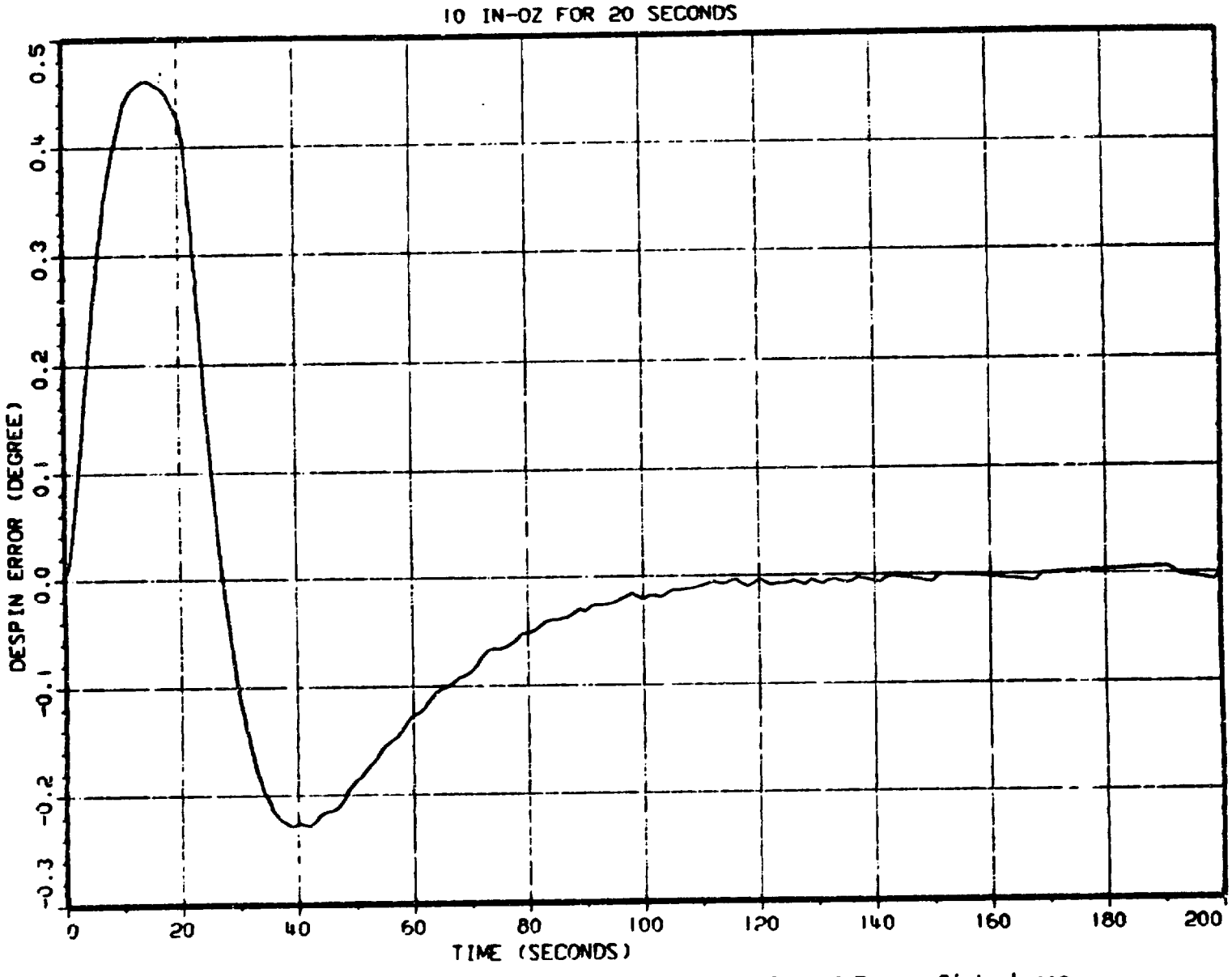

Figure 6. 9444 Response to 10 in-oz 20-second Pulse of Torque Disturbance

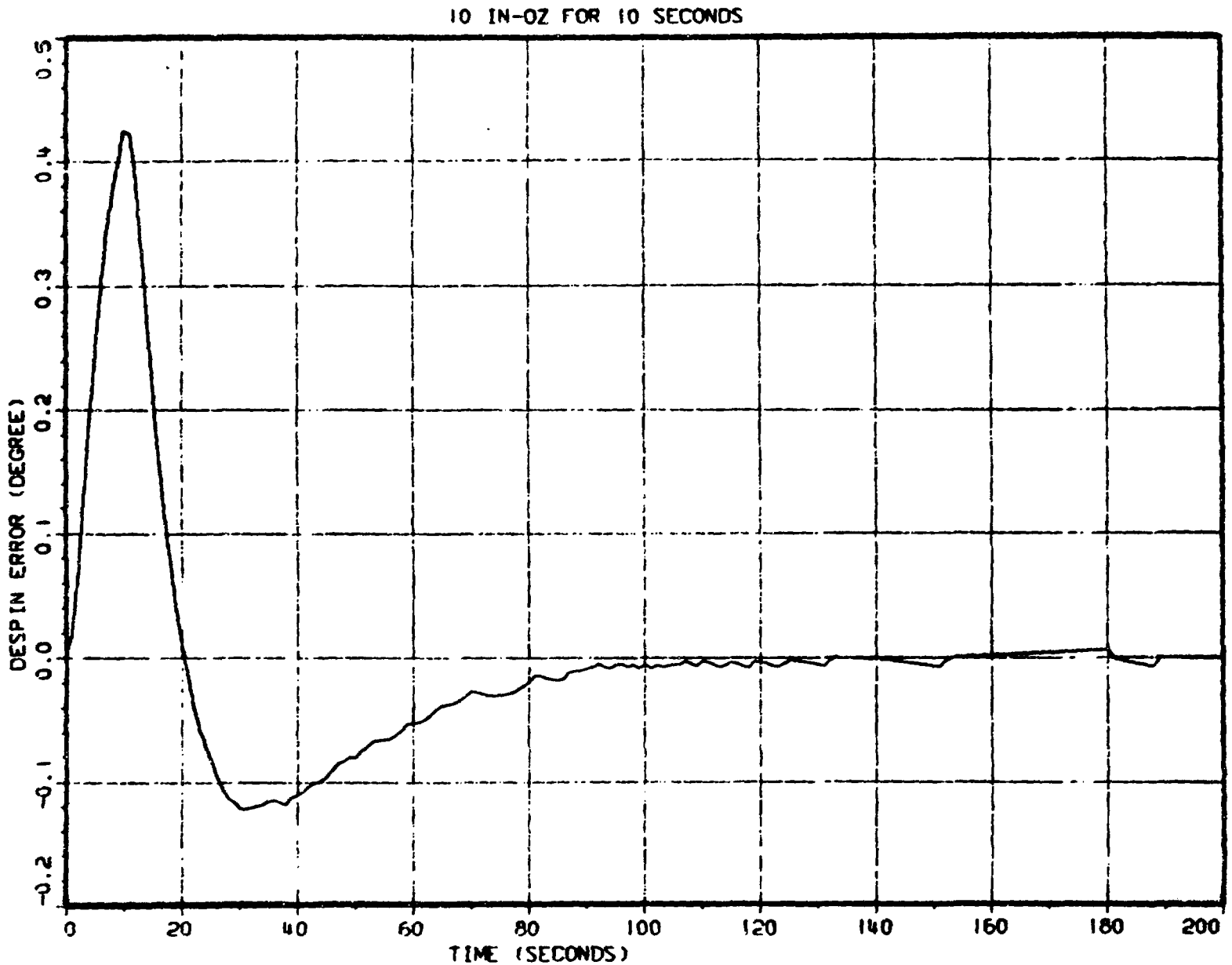

Figure 7. 9444 Response to 10 in-oz 10-second Pulse of Torque Disturbance.

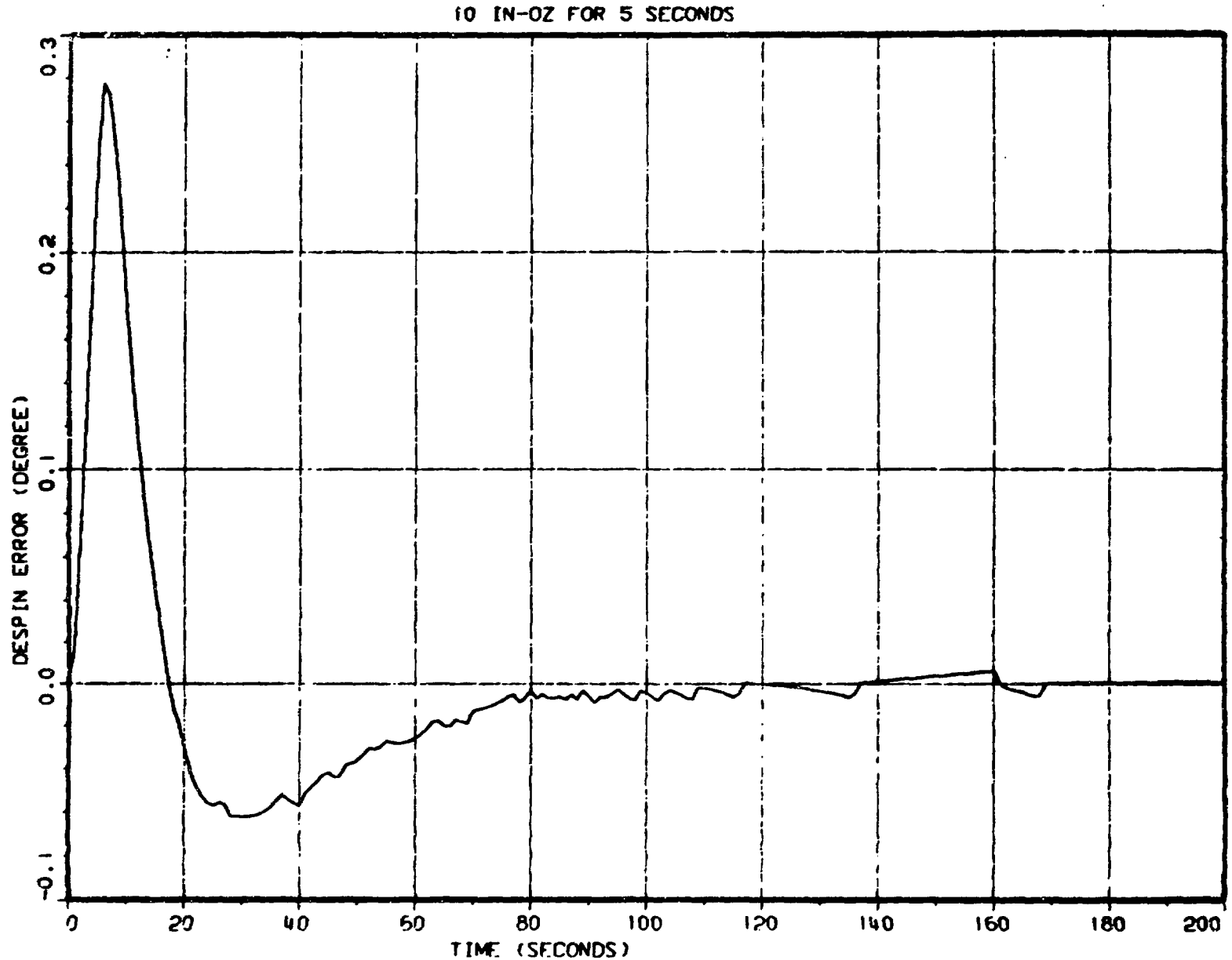

Figure 8. 9444 Response to 10 in-oz 5-second Pulse of Torque Disturbance.

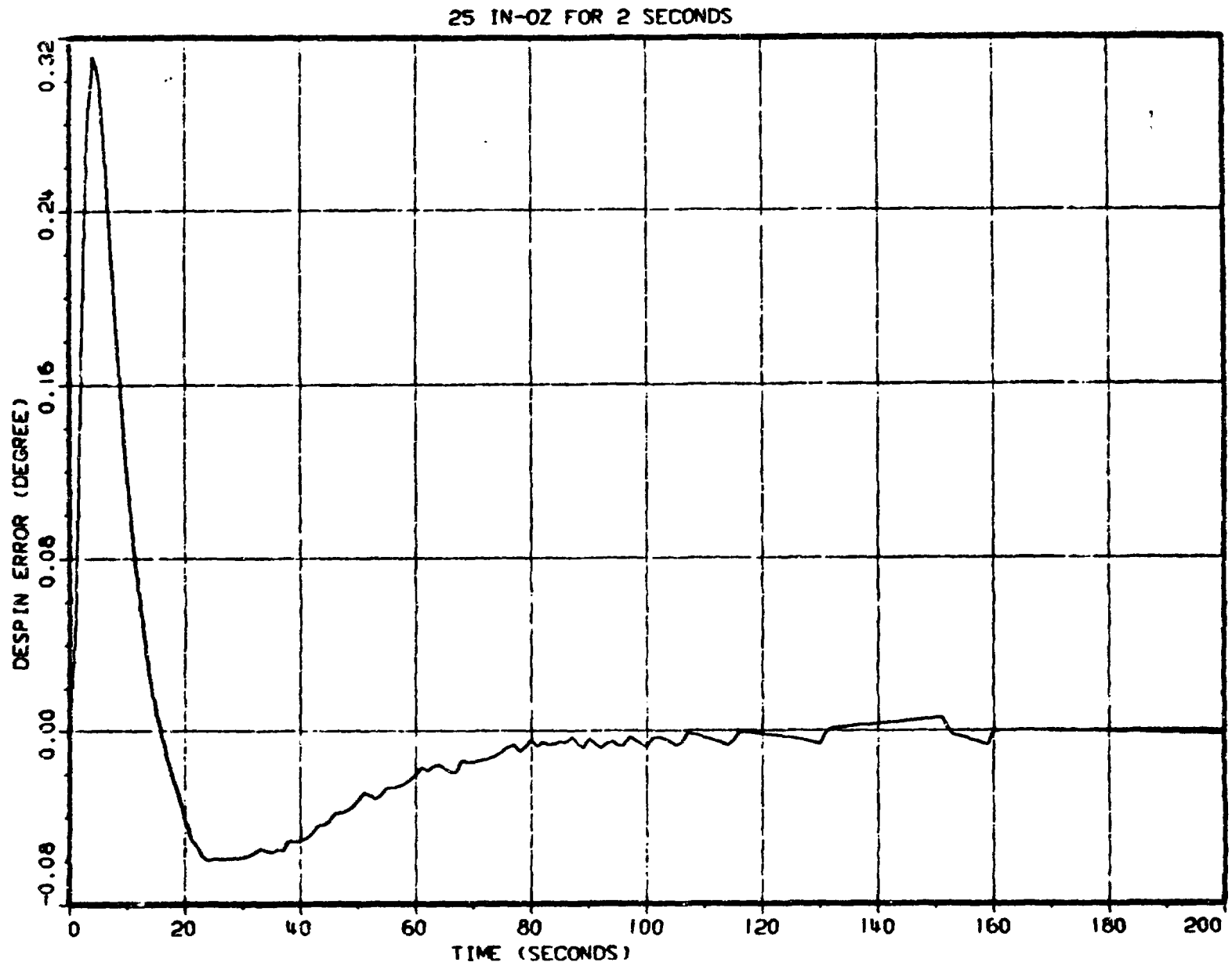

Figure 9. 9444 Response to 25 in-oz 2-second Pulse of Torque Disturbance

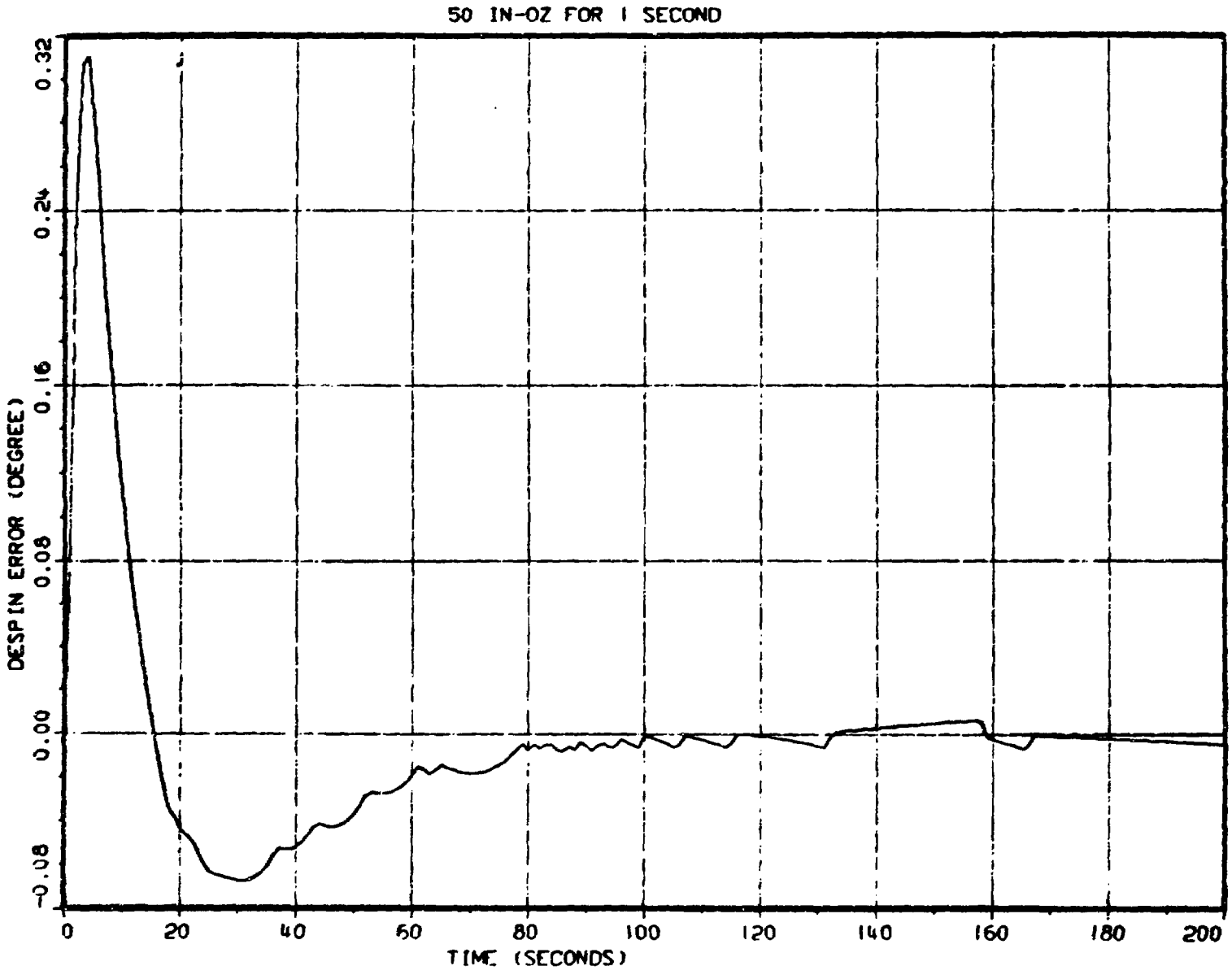

Figure 10. 9444 Response to 50 in-oz 1-second Pulse of Torque Disturbance.

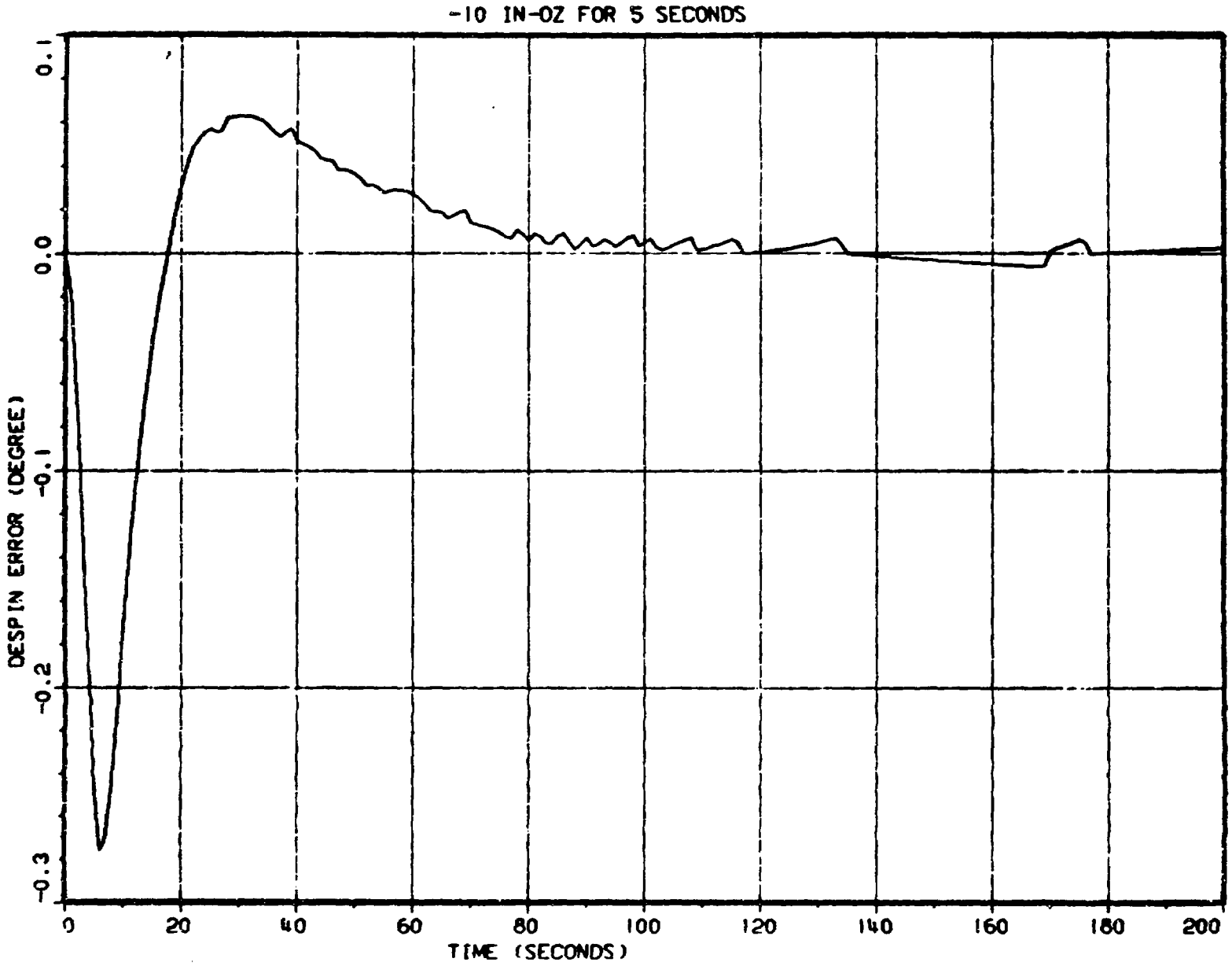

Figure 11. 9444 Response to -10 in-oz 5-second Pulse of Torque Disturbance.

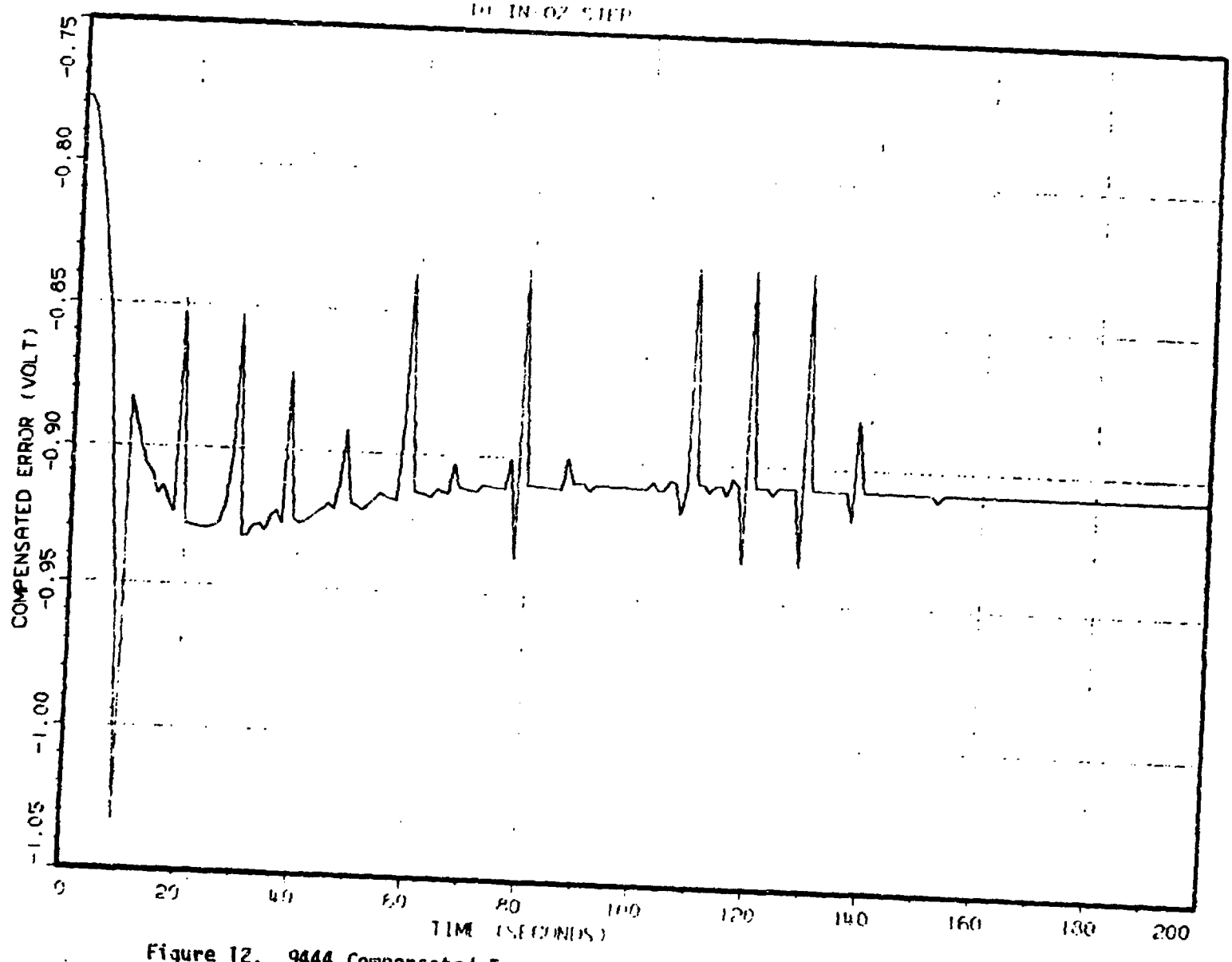

Figure 12. 9444 Compensated Error from 10 in-oz Step of Torque Disturbance. Pulses occurring after the initial transient all have the same amplitude. They all result from a one-count error, but show different amplitudes because the simulation output is not perfectly synchronized to the spinning rotor.

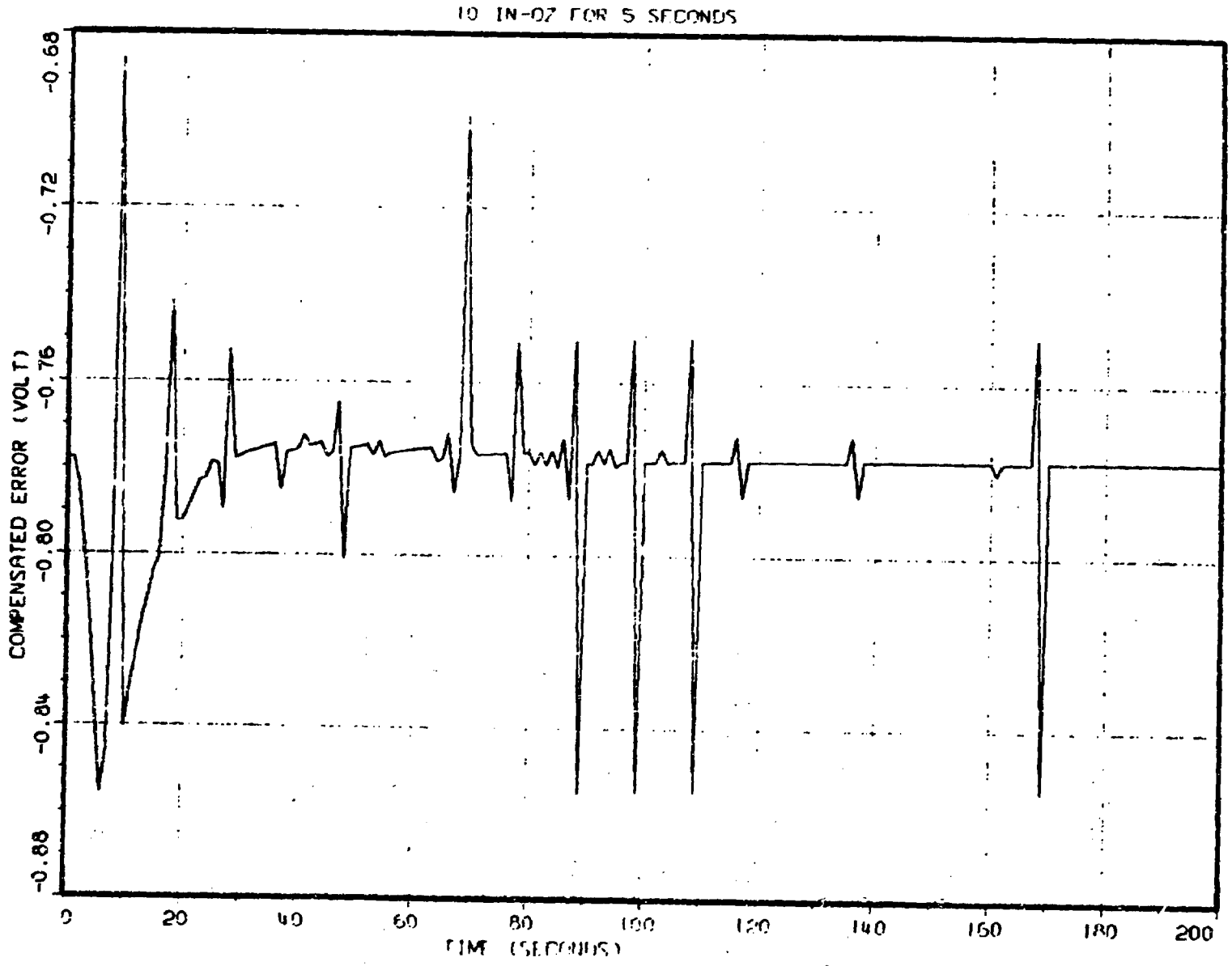

Figure 13. 9444 Compensated Error from 10 in-oz 5-second Pulse of Torque Disturbance.

Pulses occurring after the initial transient all have the same amplitude. They all result from a one-count error, but show different amplitudes because the simulation output is not perfectly synchronized to the spinning rotor.

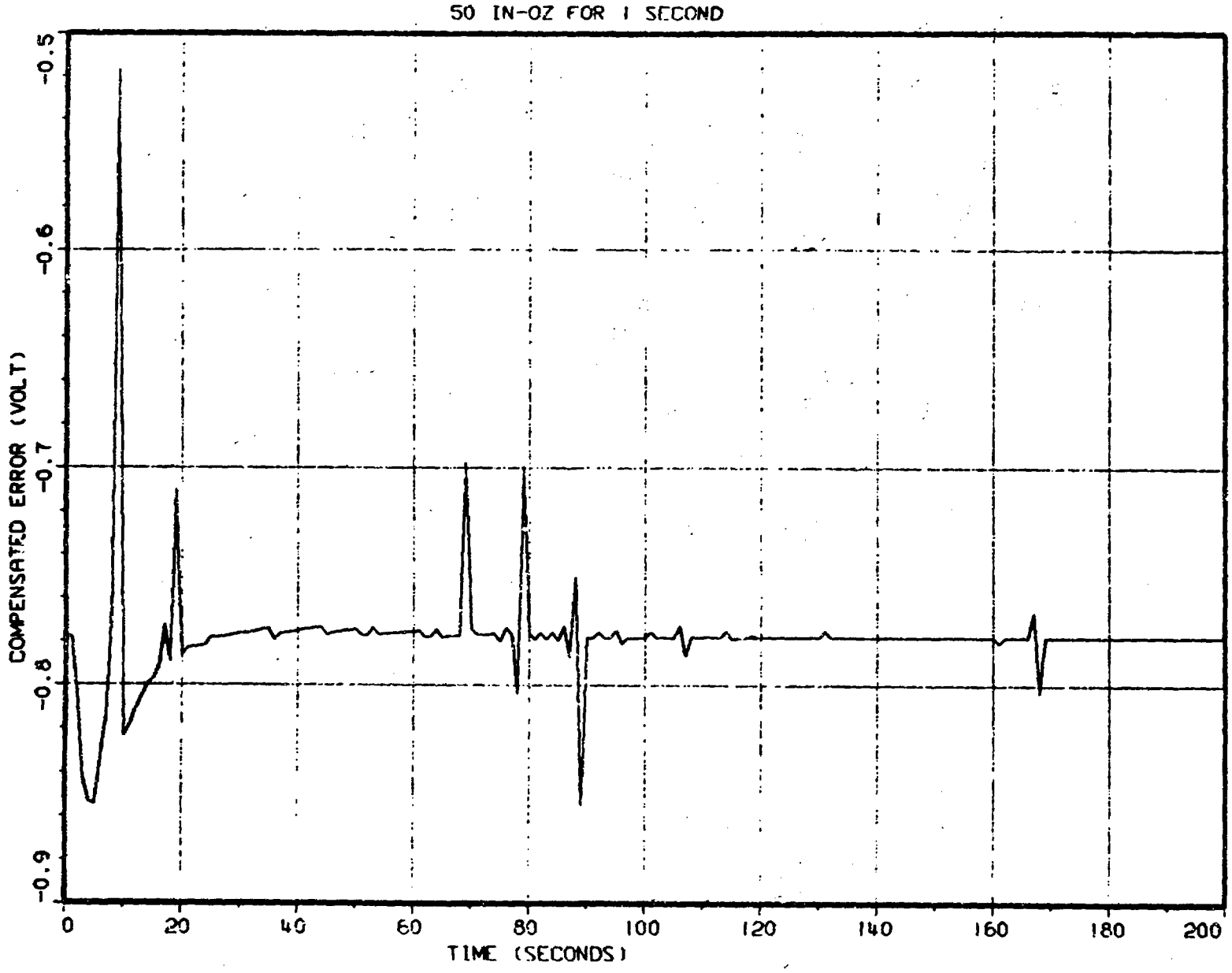

Figure 14. 9444 Compensated Error from 50 in-oz 1-second Pulse of Torque Disturbance.

Pulses occurring after the initial transient all have the same amplitude. They all result from a one-count error, but show different amplitudes because the simulation output is not perfectly synchronized to the spinning rotor.

APPENDIX II

F82-02
FINAL REPORT
DSCS II FLIGHT 14
ANOMALY INVESTIGATION

Under Contract
M27409NC1A
for
TRW
19 March 1982

Prepared By:

F. M. Manders

H. W. Davis

Approved By:

J. E. Arnold
DSCS II-DMA
Project Manager

D. A. Rogers
Electro-Mechanical
Program Manager

Aerospace Systems Division

BOULDER, COLORADO 80306

TABLE OF CONTENTS

TABLES

FIGURES

SECTION 1

INTRODUCTION

The analysis efforts described in this report were initiated because telemetry data from DSCS II Flight 14 indicated unexplainable pointing disturbances which existed sporadically. It appeared that a small sinusoidal torque disturbance with a time period of between 30 and 100 seconds was the driving function.

Under TRW Subcontract M27409NC1A, authorized by TRW TWX No. DSCS-BIF-722, BASD was directed to perform the following:

1. Analytically examine DMA bearing signatures for low frequency components in the bandwidth of 0.01 to 0.10 Hz due to geometrical characteristics.
2. Examine the characteristics of the upper bearing inner ring interfaces with respect to a radial load rotating at the DMA spin frequency (nominally 60 rpm).
3. Determine bearing frequency characteristics for a rotating radial load.
4. When initial results are obtained, a technical meeting will be held for review and to determine any additional action that should be taken.

This investigation was conducted under a T&M contract and was limited by funding. Initial plans included the examination of both the upper and lower bearings, but available funds restricted the investigation to the prescribed frequency range of the lower bearing only. This was deemed to be sufficient by TRW representatives who attended the Interim Review Meeting on 8 February 1982.

The remaining sections of this report will address the following areas:

Section 2	Basic Approach
Section 3	Detailed Analysis
Section 4	Results
Section 5	Conclusions

SECTION 2

BASIC APPROACH

Several years ago, BASD postulated that low frequency torques on the order of 0.1 Hz could be caused by bearing raceway imperfections (Interim Report on DMA Design Study, 22 February 1978, by F. M. Manders). Later, BASD measured the torque spectrum of a single bearing which did indeed show not only 0.1 Hz disturbances but several disturbance peaks in the 0.01 to 0.1 Hz region (Final Report on DMA Design Study, 13 July 1978, by F. M. Manders). Since we were primarily interested in the 0.1 Hz area, the data taken and results reported in the 0.01 Hz area may not be accurate due to the frequency reponse capability of the measuring equipment. However, the measurements do show that torque contributions appear in this lower frequency range.

The DMA performance data recently given to BASD by TRW seems to indicate a cyclic behavior occurring every 50 to 100 seconds. Since the spin rate of the drive system is about 1 Hz, this means the DMA would rotate 50 to 100 revolutions (of the shaft) for each torque cycle.

Analysis during the previous DMA Design Study indicated that torque disturbances could be in the 0.01 to 0.1 Hz range, but secondary to the prime frequency. The study was performed using geometric imperfections that were sinusoidal and symmetrical. This is not necessarily a valid assumption, and changes to this assumption could reverse the primary-secondary frequency roles.

We began this anomaly investigation by determining the number of inner ring revolutions that would produce approximately the same relative positions of both bearing rings and the ball train as were observed in the initial positions of each of the three components. This was accomplished by mathematically aligning the inner and outer rings and one ball. The position of that ball was determined for rotations of the inner ring with respect to a fixed outer ring. When the inner and outer rings were realigned and the reference ball was within the error band of being aligned, the number of inner ring rotations was noted. Figures 2-1 and 2-2 show the results of this analysis for the upper (BASD P/N 46265-3) and lower (BASD P/N 46265-1) bearings, respectively, for an error band

of ± 1 degree. Both of these figures show that for specific contact angles the number of inner ring revolutions needed to provide a ball train repeat varies from a low of 40 to a high of 300, which is in the range of interest.

If the error band is increased to one percent of a ball train revolution (±3.6 degrees) the results are as shown in Figures 2-3 and 2-4 for the upper and lower bearings, respectively. These figures narrow the number of revolutions of inner rotations for ball train repeats to the 40-80 revolution range for the contact angles analyzed.

Close examination of the preliminary satellite data indicates two predominant frequencies corresponding to about 55 and about 75 revolutions. Examinations of Figures 2-3 and 2-4 shows both frequencies are represented for both upper and lower bearings, depending on contact angle.

The upper bearing displays 56 revolutions for contact angles between 13.6 and 14.8 degrees and 74 revolutions for 11.4 to 12.2 degree contact angles. The lower bearing shows 53 revolutions for contact angles of 13.2 to 14.8 degrees and 75 revolutions from 16.2 to over 17 degrees of contact angle.

Figure 2-1

Number of Inner Ring Revolutions for Ball Train to Cycle

DMA Upper Bearing with Error Band of ± 1 Degree

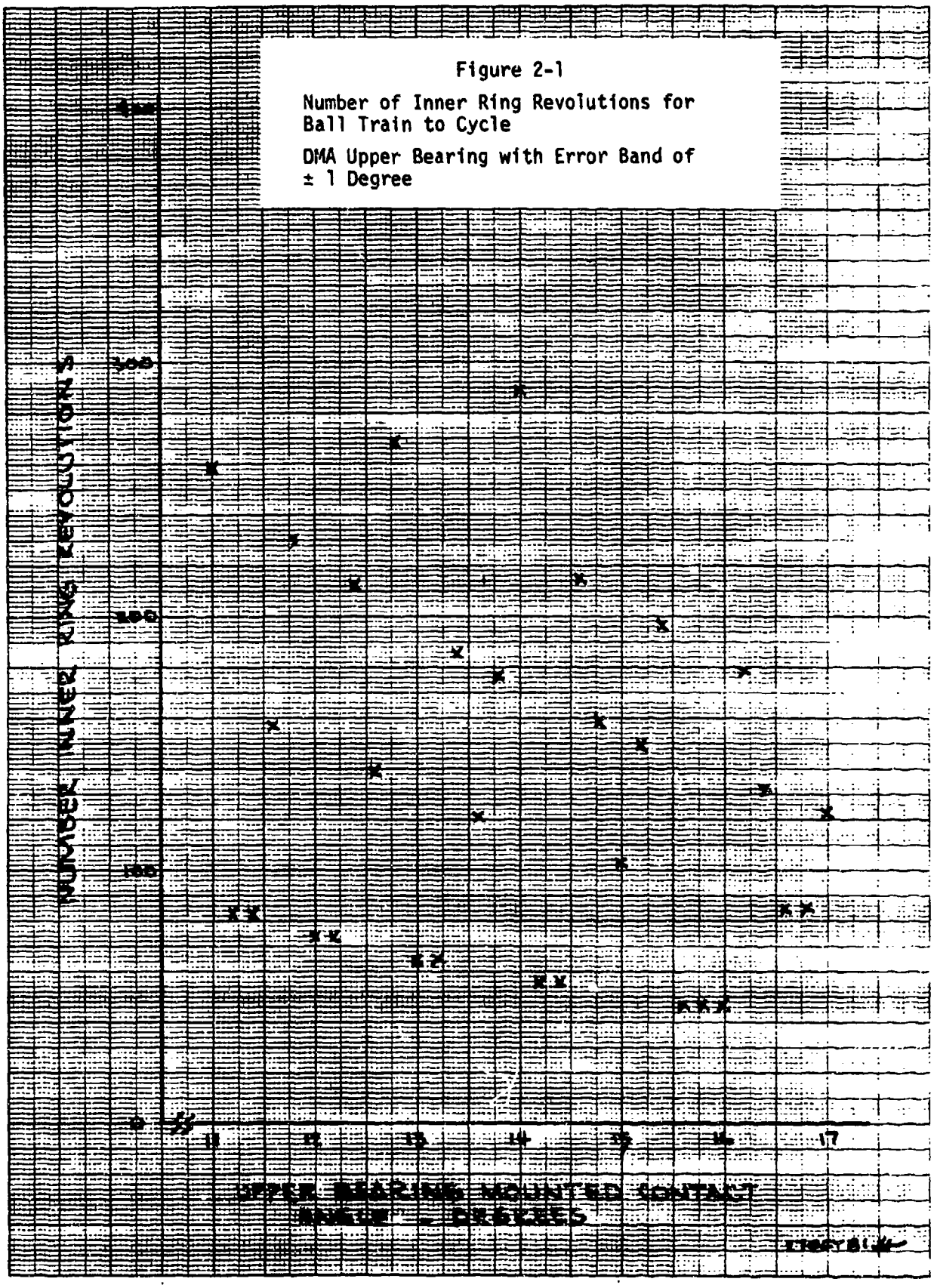

Figure 2-2

Number of Inner Ring Revolutions for Ball Train to Cycle

DMA Lower Bearing with Error Band of ± 1 Degree

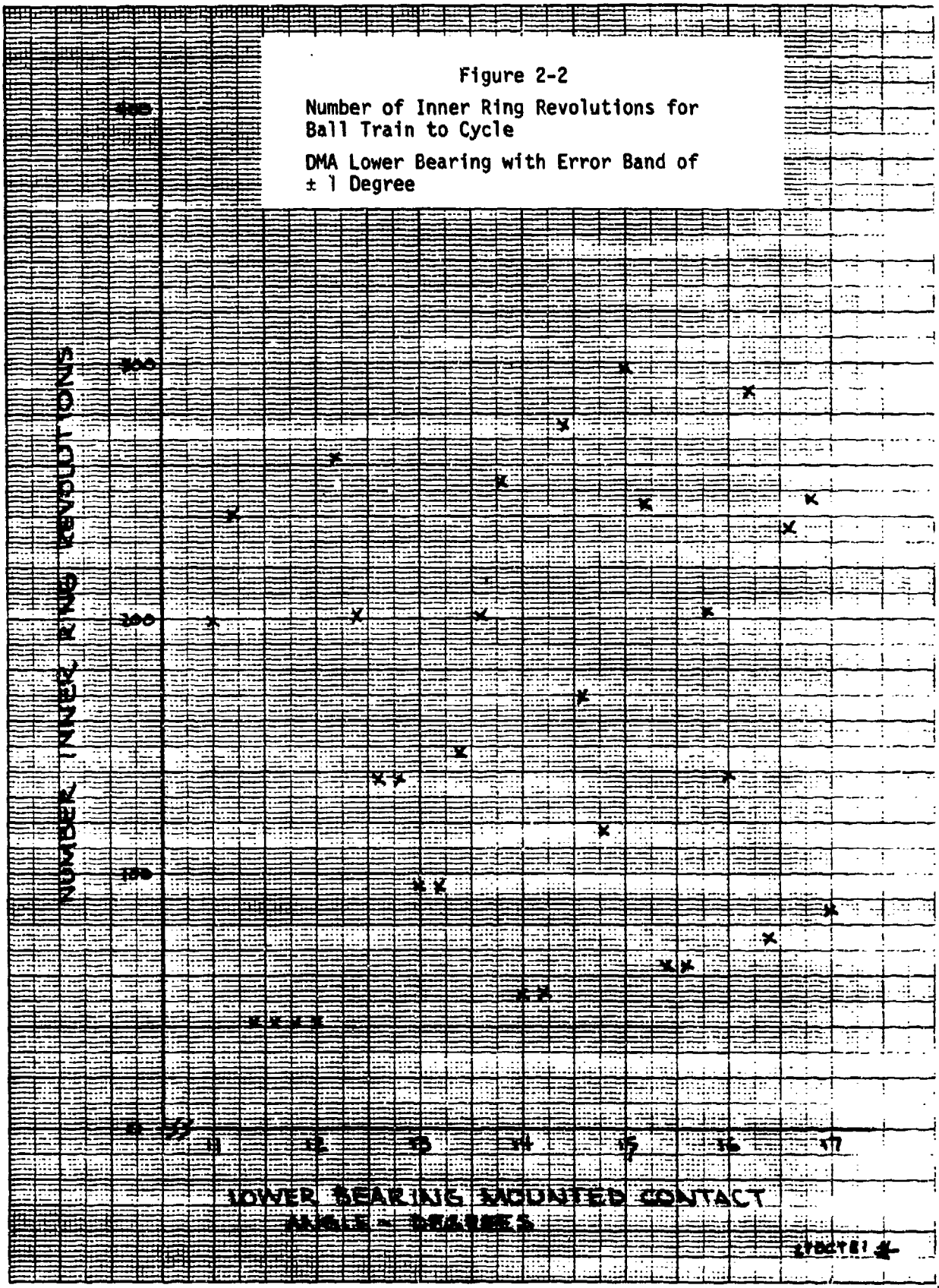

46 1513

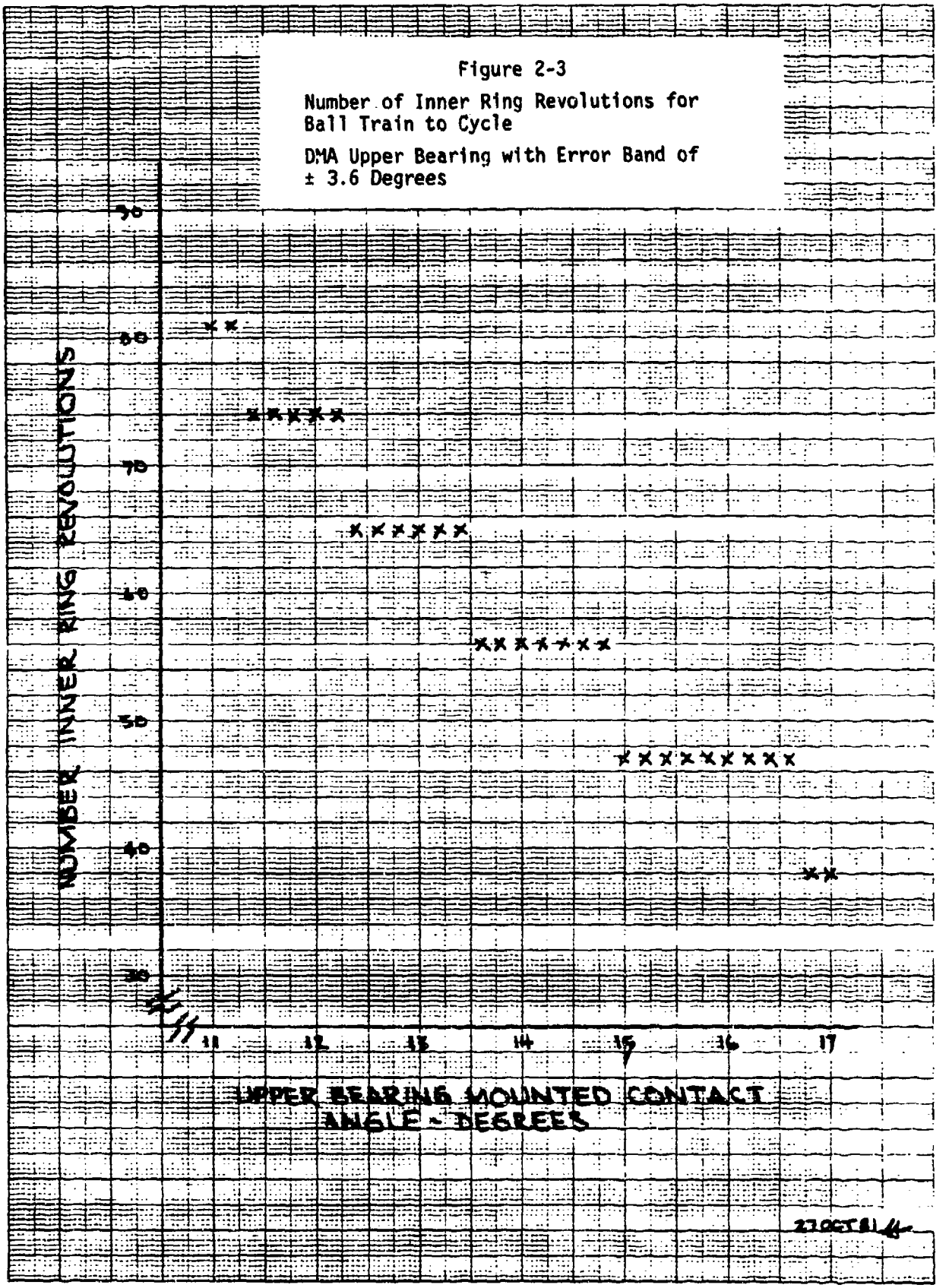

46 1513

K·E 10 X 10 TO THE CENTIMETER 18 X 25 CM KEUFFEL & ESSER CO

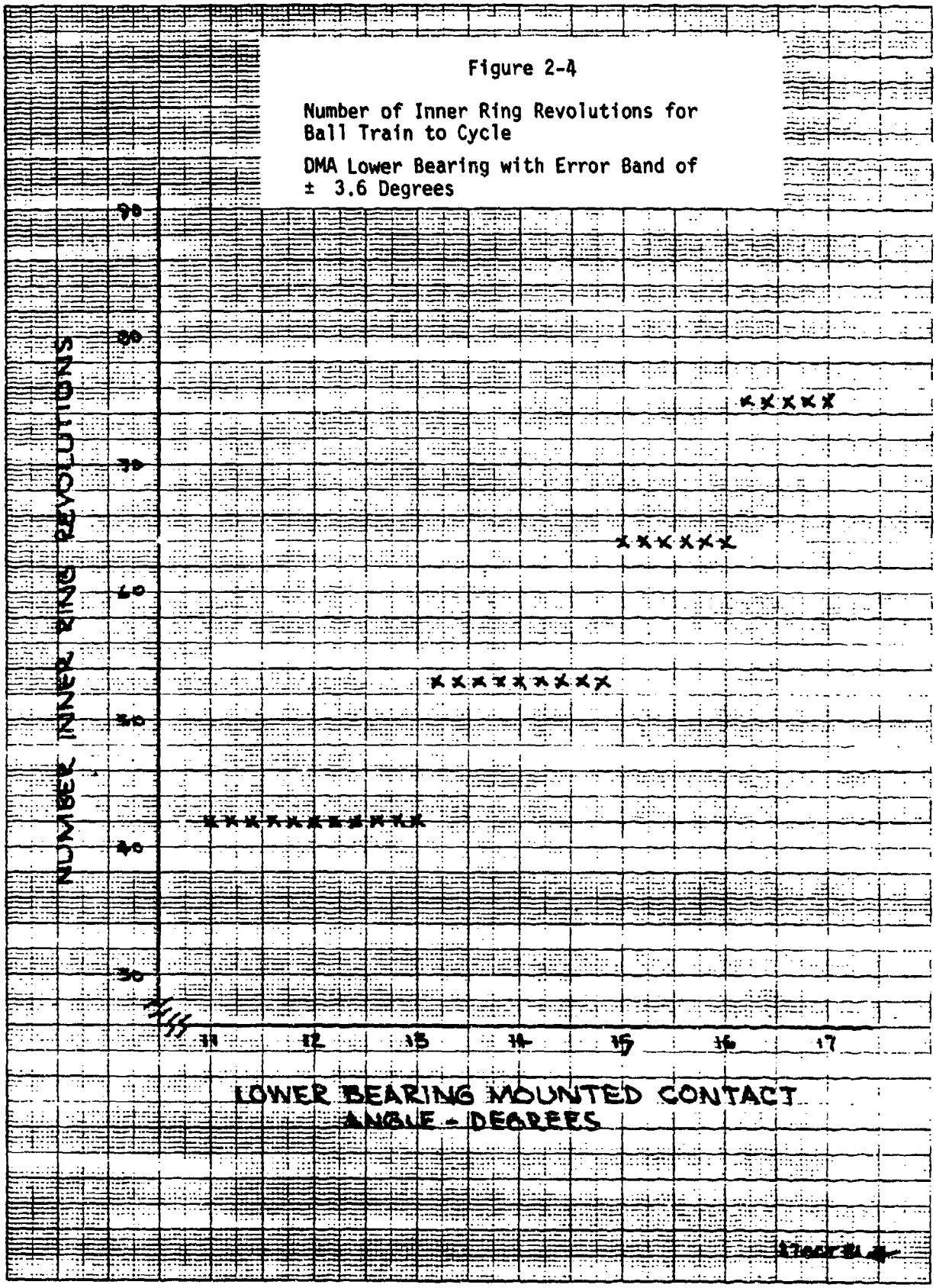

SECTION 3

DETAILED ANALYSIS

As a result of the 1978 DMA Design Study, BASD developed some equations for ball speed variation (BSV) displacement effects. That theoretical development was changed slightly to allow actual bearing parameters to be incorporated into the analysis for the present anomaly investigation. The present analysis incorporated the results from the previous study and defined bearing parameters to arrive at the total results of BSV displacement. These four contributing factors are:

1. Ball diameter variation
2. Bearing misalignment
3. Bearing raceway geometry variation
4. Rotating radial load effects

3.1 Ball Speed Variation (BSV) Displacement Assumption

BSV displacements are defined as the differential distance traveled by a particular ball due to one or more of the above factors when compared to a ball/race interface with nominal characteristics. We have seen that bearing balls will actually be either advanced or retarded with respect to perfect bearing condition. These changes will cause pinching of the ball cage (retainer) between the most advanced ball and the most retarded ball. As the ball-to-cage forces increase, the retainer force on the ball will eventually become large enough to overcome the ball-to-race normal force times the coefficient of friction and at least one of the cage-contacting balls will slide back into the ball pocket. Another ball will pick up the chase and the process repeats. This action becomes one of the components of bearing internal torque. It was BASD's intention to work with a simplified model to establish a basis for predicting the 0.01 to 0.1 Hz frequencies and then, if possible, to generate the model for this, the torque-producing cage interface contact.

We next investigated the costs involved with examining each ball and performing analysis on that information. After some consideration BASD decided to attack the problem by summing the BSV displacements of all balls, collapsing more than twenty data points (one for each ball) down to one. Thus, the sum value

represents the net displacement and is found by adding the individual displacements of each ball.

While BASD does not expect this to be a real physical condition, it does provide the frequency logic of the bearing examined.

3.2 Analysis Methodology

Each of the following previously named factors has an effect upon the internal radial clearance of a bearing:

1. Ball diameter variation (Case 1)
2. Bearing misalignment (Case 2)
3. Bearing raceway geometry variation (Case 3)
4. Rotating radial loads effects (Case 4)

To analyze BSV displacement effects due to all four factors, it is necessary to first calculate radial clearance due to each factor and sum them.

$$C_{r_t} = C_{r_1} + C_{r_2} + C_{r_3} + C_{r_4} \tag{3.1}$$

The resultant radial clearance can be used to calculate a resultant value for the bearing contact angle (β).

$$\cos \beta = 1 - \frac{C_{r_t}}{Bd} \tag{3.2}$$

where B = Total curvature

d = Ball diameter

Knowing beta, the angular travel of the ball (and ultimately the linear travel of the ball) can be calculated. Inner ring rotation was limited in this analysis to small (one degree) increments, such that $\tan \Theta_{r_j} \approx \Theta_{r_j}$.

$$\Theta_{b_j} = 1/2 \left(1 - \frac{d_n \cos\beta}{E}\right) \tag{3.3}$$

$$\Delta S_{BSV} = \frac{E}{2} \quad (\Theta_{b_i} - \Theta_{b_n}) \tag{3.4}$$

where d_n = Diameter of the nominal ball

Θ_{b_n} = Angular travel of the nominal ball

ΔS_{BSV} = Incremental linear travel of the ball in question.

Therefore, the total linear distance traveled is:

$$S_{BSV} = (S_{BSV})_{Previous} + \Delta S_{BSV} \tag{3.5}$$

The analysis task is now reduced to one of calculating the internal radial clearances due to each applicable factor. The methods used for each factor will be described separately in the following paragraphs.

Using this methodology and the bearing characteristics of the lower DMA bearing (P/N 46265-1), as shown in Table 3-1, plots of BSV displacements were generated for each of the four factors.

Table 3-1
Characteristics of the DMA
Bearing No. 46265-1 per BASD Analysis

BEARING PARAMETER	VALUE
Nominal Ball Diameter, d_n	0.5000 in
Ball size variations, t	(see Table A-1)
No. of Balls, n	23
Precision (assumed)	AFBMA Grade 5
Nominal contact angle, β_n	14.0
Maximum contact angle due to misalignment, β_m	14.5^0
Maximum contact angle due to rotating loads, β_o	15.0^0
Pitch Diameter, E	5.14 in
Outer Race Curvature, f_o	0.5275
Inner Race Curvature, f_i	0.5175

3.3 Ball Diameter Variation (Case 1)

Particular values were assumed for individual ball diameters. These values were randomly selected, based upon a normal distribution of diameter variations and assuming an AFBMA Grade 5 bearing. This resulted in a set of deviations which were symmetrical about the zero value. These variations in diameter produced displacements which were linear and symmetrical about the nominal value. Therefore, the sum of the BSV displacements due only to ball diameter variations had a net effect of zero. The assumed values of ball diameter variations used in this analysis are listed in Appendix A.

Internal radial clearance for a ball of nominal diameter and assuming a perfect circular raceway is:

$$C_{r_n} = Bd_n\ (1 - \cos\beta_n) \tag{3.6}$$

For any other ball, whose diameter differs from nominal by an amount t, the diameter is

$$d_i = d_n + t_i \tag{3.7}$$

and the internal radial clearance is:

$$C_{r_i} = Bd_i\ (1-\cos\beta_i) \tag{3.8}$$

and

$$C_{r_i} = C_{r_n} - t_i \tag{3.9}$$

so

$$C_{r_i} = Bd_n\ (1-\cos\beta_n) - t_i \tag{3.10}$$

This value becomes C_{r_1} in equation (3.1). The diameter deviation t is known for each ball and the rest of the parameters on the righthand side of equation (3.10) are constants. Thus, C_{r_1} is constant for a particular ball and the BSV displacements for that ball are linear. This analysis assumes no interface contact between balls and retainer, and further assumes no skidding of the balls with respect to the races.

3.4 Bearing Misalignment (Case 2)

It is very difficult to mount a bearing in such a way as to produce no relative angular misalignment between rings. This angular misalignment will produce a

varying contact angle which can be closely approximated by a sinusoid.

$$\beta_2 = \beta_n + (\beta_m - \beta_n)\ \cos(\Theta_{b_{av}} + \Theta_{b_{tp}} + \Theta_i) \qquad (3.11)$$

where β_2 = the instantaneous contact angle due to misalignment

β_n = the nominal contact angle

β_m = the maximum contact angle

Θ_i = initial angular position of each ball

$\Theta_{b_{av}}$ = incremental angular position of the ball

$\Theta_{b_{tp}}$ = previous value of the angular location of each ball as a result of an inner ring rotation Θ_{r_i}

This analysis assumed the characteristics of the lower DMA bearing (P/N 46265-1) with a 63 pound preload. It also assumed a relative angular misalignment (α) of inner and outer races equal to 0.00007 radians, which results in a maximum contact angle $\beta_m = 14.5^{o}$. The internal radial clearance, C_{r_2}, due to misalignment is:

$$C_{r_2} = Bd_n\ (1-\cos\beta_2) - C_{r_n} \qquad (3.12)$$

3.5 Bearing Raceway Geometry Variation (Case 3)

The analysis of raceway geometry effects makes use of an actual raceway profile taken from bearing inspection data and provided to BASD by the Fafnir Bearing Company. This data was used to develop an algorithm which relates half-height dimensions of inner and outer race lobes (HI and HO) to some angular location Ψ on the raceway.

In developing this algorithm, no attempt was made to duplicate exactly the prescribed bearing geometry profile. The objective here was to recreate the general form of the geometry profile, which was noted to be neither symmetrical nor purely sinusoidal.

For the inner race,

$$\Psi_i = \Theta_i + \Theta_{b_{av}} + \Theta_{b_{tp}} - \Theta_{r_i} \tag{3.13}$$

where

Ψ_i = some angular location

Θ_{r_i} = angular location of the inner ring

Values of Ψ_i are used in the following algorithm to determine half-height dimensions for the inner race.

$$\begin{aligned} HI = 2 \times 10^{-6} \{ & H_1 \sin \Psi_i + H_2 \sin 2\Psi_i + H_3 \sin 3\Psi_i \\ & + H_4 \sin 4\Psi_i + H_5 \cos \Psi_i + H_6 \cos 2\Psi_i \\ & + H_7 \cos 3\Psi_i + H_8 \cos 4\Psi_i \} \end{aligned} \tag{3.14}$$

where $H_1 - H_8$ are predefined constants.

For the outer race,

$$\Psi_o = \Theta_i + \Theta_{b_{av}} + \Theta_{b_{tp}} \tag{3.15}$$

and

$$\begin{aligned} HO = 2 \times 10^{-6} \{ & H_1 \sin \Psi_o + H_2 \sin 2\Psi_o + H_3 \sin 3\Psi_o \\ & + H_4 \sin 4\Psi_o + H_5 \cos \Psi_o + H_6 \cos 2\Psi_o \\ & + H_7 \cos 3\Psi_o + H_8 \cos 4\Psi_o \} \end{aligned} \tag{3.16}$$

The internal radial clearance due to raceway geometry variations,

$$C_{r_g} = HI + HO \tag{3.17}$$

Details of the specific algorithm used in this analysis are included in Appendix B.

3.6 Rotating Radial Load Effects (Case 4)

The rotating radial load analysis assumed that a radial load of approximately 15 pounds acts upon the inner ring in a direction which is fixed with respect to the inner ring. This radial load in combination with the 63 pound axial preload on the lower DMA bearing resulted in a relative angular misalignment of α = .00011 radians between the inner and outer rings.

Assuming sinusoidal variations in contact angle due to the rotating load, as was done for bearing misalignment (Case 2), we find that the contact angle varies about the nominal value of 14.0^{o} to a maximum of almost 15^{o}. The contact angle variations are described by

$$\beta_4 = \beta_n + (\beta_0 - \beta_n) \cos \Psi_j \qquad (3.18)$$

where β_4 = the instantaneous contact angle due to rotating loads effects

β_0 = the maximum contact angle

Ψ_j = the angle defined by equation (3.13)

The internal radial clearance, C_{r_4}, due to rotating radial load effects is

$$C_{r_4} = Bd_n (1-\cos \beta_4) - C_{r_n} \qquad (3.19)$$

3.7 Sum of Cases (2 + 3 + 4)

As explained in Section 3.1 of this report, BASD decided to attack the analysis problem by summing the BSV displacements of all balls. This summation produced a net displacement value for the total bearing, and later demonstrated a marked similarity to previously observed bearing performance data. Displacements due to ball diameter variation, Case 1, were not included in the calculations of sum values because it was apparent that the sum of these displacements had a net effect of zero.

To determine these summation values, the value of BSV displacement due to Cases (2 + 3 + 4) was calculated for each ball and this was summed for every ball in the bearing.

$$SUM = \sum_{i=1}^{n} (S_{BSV})_i \qquad (3.20)$$

SECTION 4

RESULTS

4.1 Ball Diameter Variation (Case 1)

BSV displacements due only to variations in ball diameter are linear functions, as shown in Figure 4-1. Therefore, when ball diameter variations are considered in conjunction with other factors (i.e. misalignment, raceway geometry variation, and rotating radial load effects), they introduce a linear bias for each ball with a slope dependent upon the magnitude of the diameter variation. Since this effect was predictable, ball diameter variations were neglected in most analyses in order to simplify the results and reduce the magnitude of the total displacements. This did not detract in any way from the validity of the analysis results. In addition, the net effect of ball diameter variations upon the value of SUM was zero, because of the normal distribution and the symmetrical characteristics of the particular values which were assumed, as shown in Figure A-1.

4.2 Bearing Misalignment (Case 2)

BSV displacements due only to misalignment produce a trace for each ball that is sinusoidal in shape and of a constant frequency, as shown in Figure 4-2. For the assumed values of nominal contact angle (β_n = 14.0°), maximum contact angle (β_m = 14.5°) and rotation speed (60 RPM), this frequency is 0.451 Hz.

As might be expected, BSV displacements are both cyclic and symmetrical. The same ball achieves the maximum positive displacement value in each cycle because it is a function of the initial angular position, Θ_i, of the ball within the ring. Also, a slight upward bias was noted in the BSV displacement plots.

4.3 Bearing Raceway Geometry Variation (Case 3)

BSV displacements due only to raceway geometry variation produce a trace for each ball that is cyclic in nature but which exhibits drastic variations in the amplitudes of maxima and minima. Although the individual cycles are somewhat difficult to define, they appear to have a period of approximately 0.500 Hz. This is shown in Figure 4-3.

The same ball does not achieve maximum displacement in every cycle. In general, the maximum displacements caused by raceway geometry variations are an order of magnitude smaller than the maximum displacements due to either misalignment or rotating load effects.

4.4 Rotating Radial Load Effects (Case 4)

BSV displacements due only to rotating radial loads produce a trace for each ball that is sinusoidal in shape and of a constant frequency, as shown in Figure 4-4. For the assumed values of nominal contact angle (β_n = 14.0°), maximum contact angle (β_o = 15.0°) and rotation speed (60 RPM), this frequency is 0.548 Hz.

This plot resembles Figure 4-2 (Misalignment), in that the same ball achieves the maximum positive displacement value in each cycle and for the same reason. Also, a slight upward bias was noted in this plot, too.

4.5 Sum of Cases (2 + 3 + 4)

The sum of BSV displacements for all balls and due to the composite factors of Cases (2 + 3 + 4) produced a trace that was apparently a straight line, as shown in Figure 4-5. However, detailed examination of the numerical data suggested that these SUM values actually produced minor high-frequency variations which were too small to be discernable on the plot. This fact was later substantiated by using the method of least squares to eliminate the uniform bias and by plotting the remaining data variations, as shown in Figure 4-6. Eliminating this bias did not degrade the results of this analysis because we were primarily interested in determining frequencies rather than displacement magnitudes.

4.6 Bias Effects

As previosly mentioned, the plots of Case 2 (Misalignment), Case 4 (Rotating Radial Loads) and the Composite Case (2 + 3 + 4) all exhibited a positive linear bias. Plots of the SUM values for each of these separate conditions also exhibited a positive bias. Case 3 SUM (Raceway Geometry Variation) had a negative bias which appeared to be almost (but not quite) linear. During the initial stages of this analysis effort, it was suspected that these bias effects were caused by one or more of the following:

1. Round-off errors
2. Errors due to assuming that the angle Θ is approximately equal to tan Θ for small values of Θ
3. Errors due to iterative procedures wherein the final solution is always approached from the same direction (i.e. positive or negative).

However, further study has convinced us that the bias effect is a valid one, at least for Cases 2 and 4. The values of the angles used in this analysis are so small that the angle and the tangent are identical out to 10 decimal places. Also, the error differential used to terminate iteration is so small (5×10^{-6}) that round-off errors are insignificant. The remaining cause (i.e. errors due to iterative procedures) was also dismissed after manually performing the calculation and noting that the current procedures minimize the amount of bias. It was further noted that equal positive and negative changes in the contact angle, β, produce unequal changes in the cosine β term. This fact seems to account for the positive bias and can be demonstrated numerically.

4.7 Revised Sum

The term "revised Sum" refers to the plot of summation values for Cases (2 + 3 + 4) after the linear bias has been eliminated. This is shown in Figure 4-6, where 100 seconds of data are plotted.

Visual exaimination of Figure 4-6 showed that the SUM values vary in a periodic manner and that several predominant frequencies can be identified. In the frequency range of interest (0.01 Hz to 0.10 Hz), this cyclic behavior was noted at 0.019 Hz, 0.024 Hz, 0.034 Hz, 0.082 Hz, and 0.100 Hz.

This is illustrated in Figures 4-7 through 4-11, where matching numerals are used to denote cycle peaks on top of the curve and matching letters are used to denote cycle peaks below the curve.

4.8 Frequency Analysis

In an effort to better define the frequency spectra for the revised SUM data, a Fourier analysis was accomplished by using the IMSL routine FFTRC. This

routine computes the fast Fourier transform of a real-valued sequence of N data points and outputs a complex vector of length (N/2) + 1 containing the first (N/2) + 1 coefficients of the Fourier transform.

Having recorded data points for SUM every 10 degrees for 100 revolutions (3600 total), the output contained 1801 values. The frequency interval Δf is predetermined by the total time interval represented by the original data, such that

$$\Delta f = \frac{1}{T} = \frac{1}{N\Delta t} \qquad (4.1)$$

where Δf = minimum frequency interval of the Fourier transform
Δt = time interval of the original data
N = Number of points in the original data
T = Total time span of the original data

Since the SUM data covered a span of 100 seconds, the minimum frequency interval of the Fourier transform is 0.01 Hz and the maximum frequency analyzed and displayed is 18.00 Hz. Plots of the resulting Fourier transform are shown in Figures 4-12 and 4-13.

There is good correlation between the transform value peaks shown in Figure 4-13 and the predominant frequencies found by visual inspection of Figure 4-6.

Figure 4-1 BALL SIZE VARIATIONS

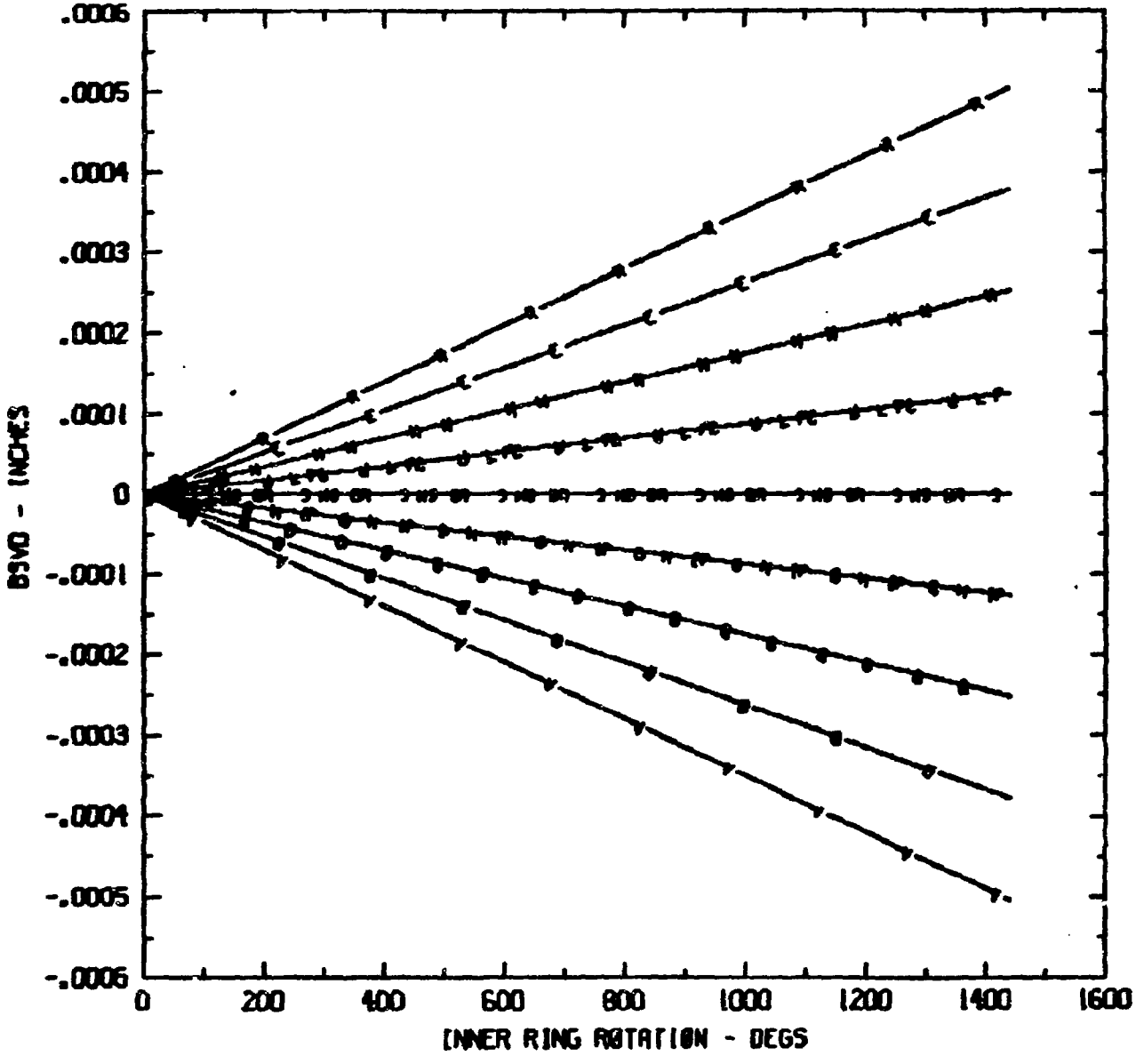

Figure 4-2 MISALIGNMENT

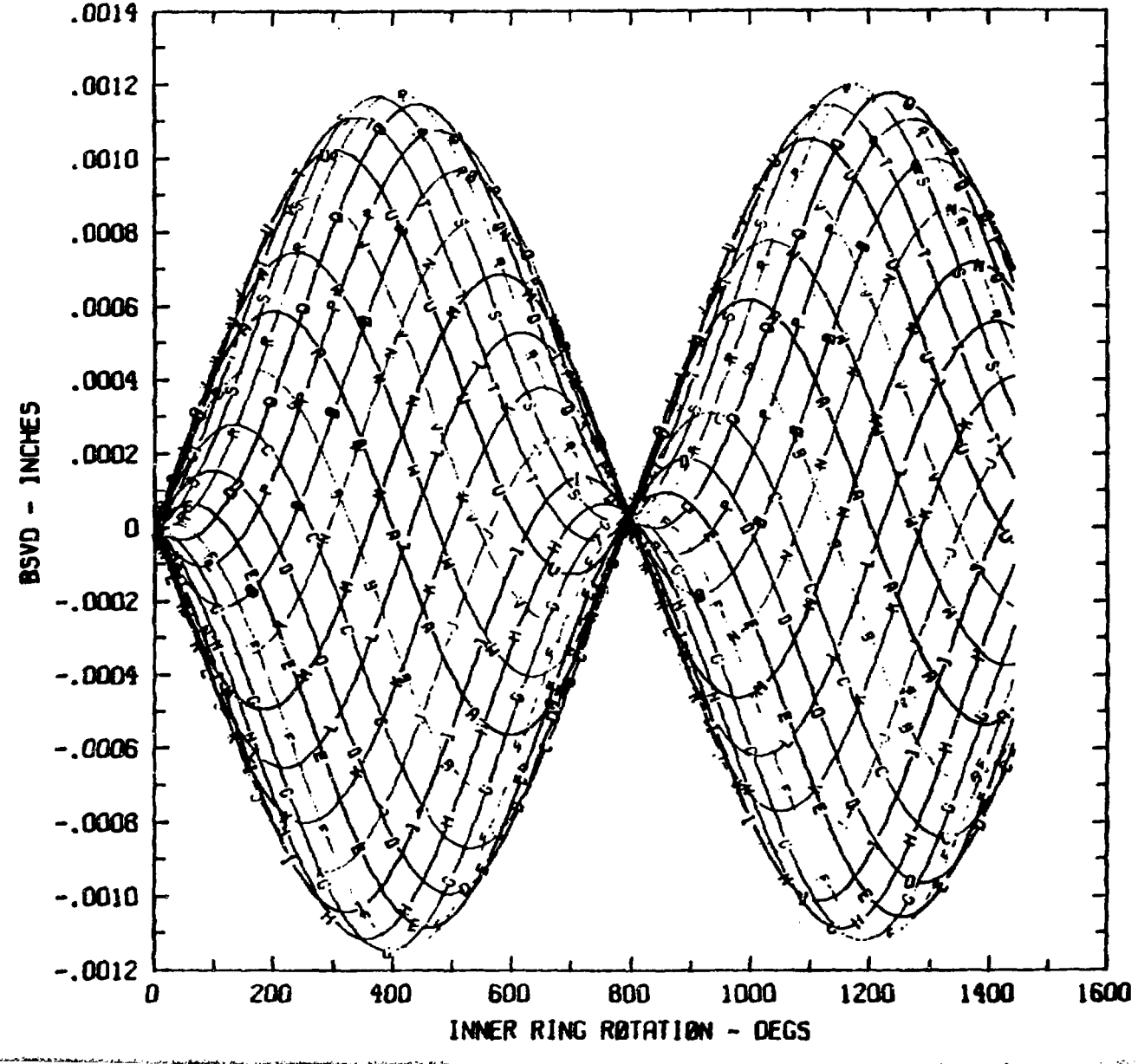

Figure 4-3 RACEWAY IMPERFECTIØNS

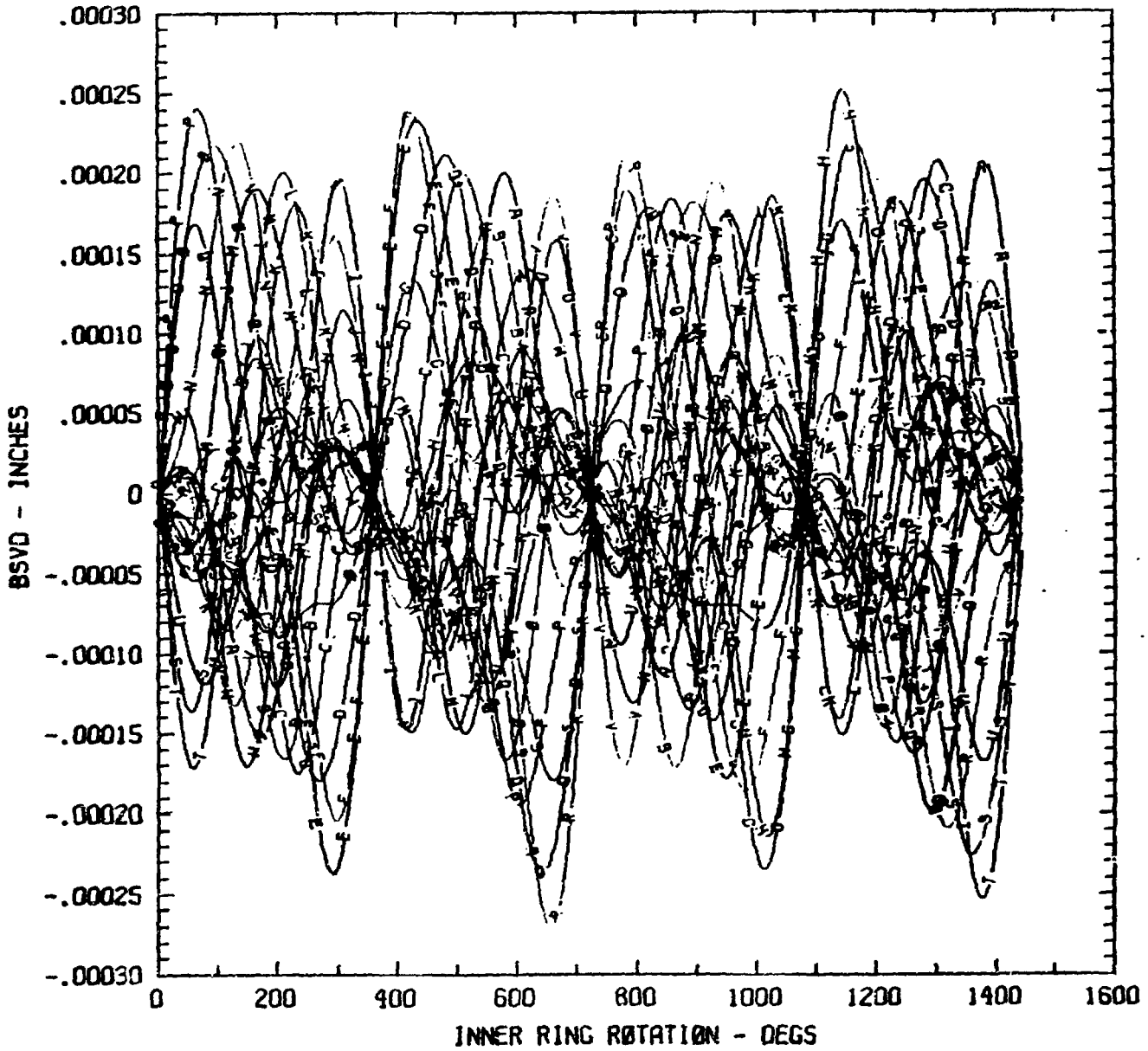

Figure 4-4 RØTATING LØADS

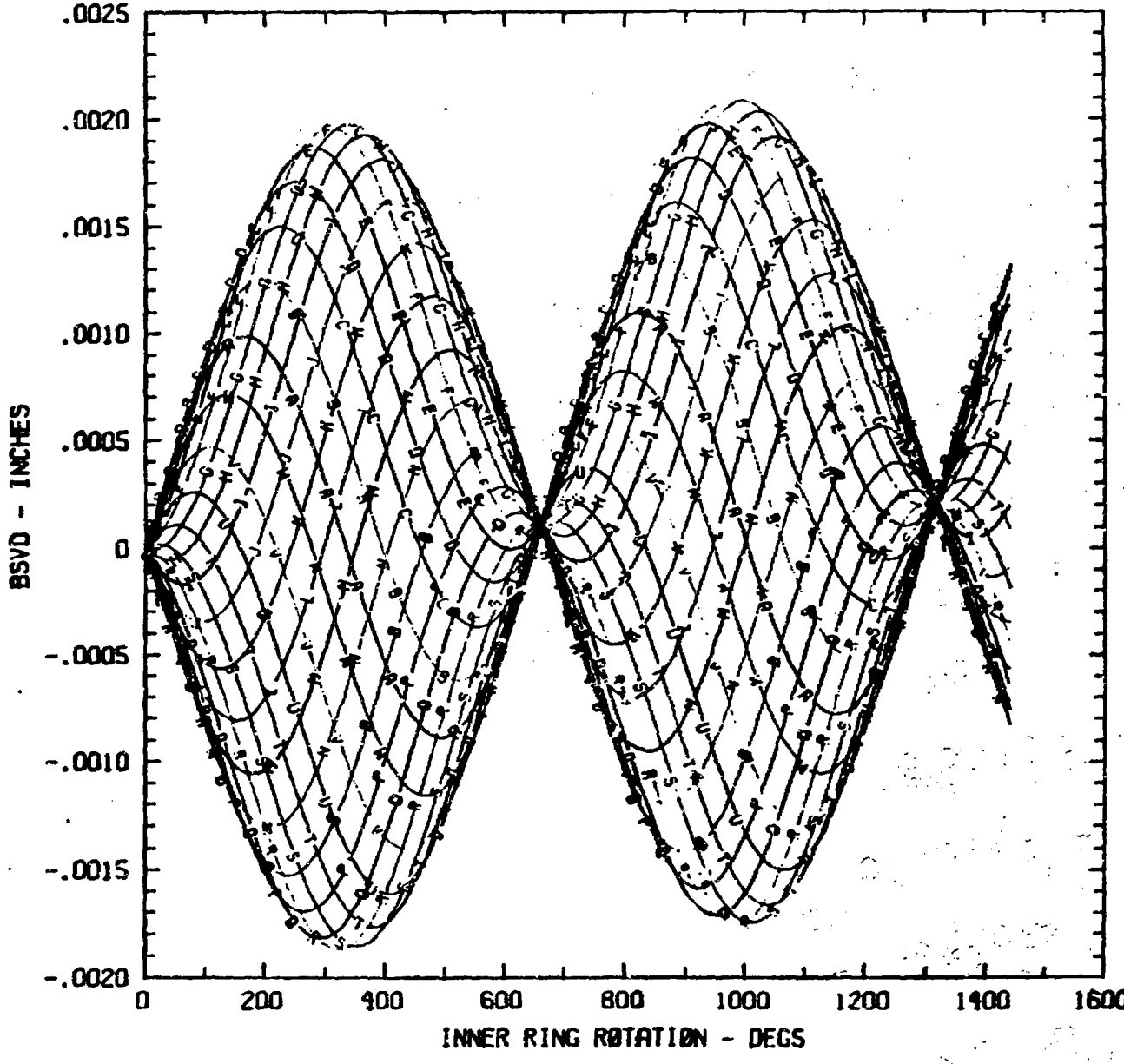

Figure 4-5 BSVD SUM (FACTØRS 2+3+4)

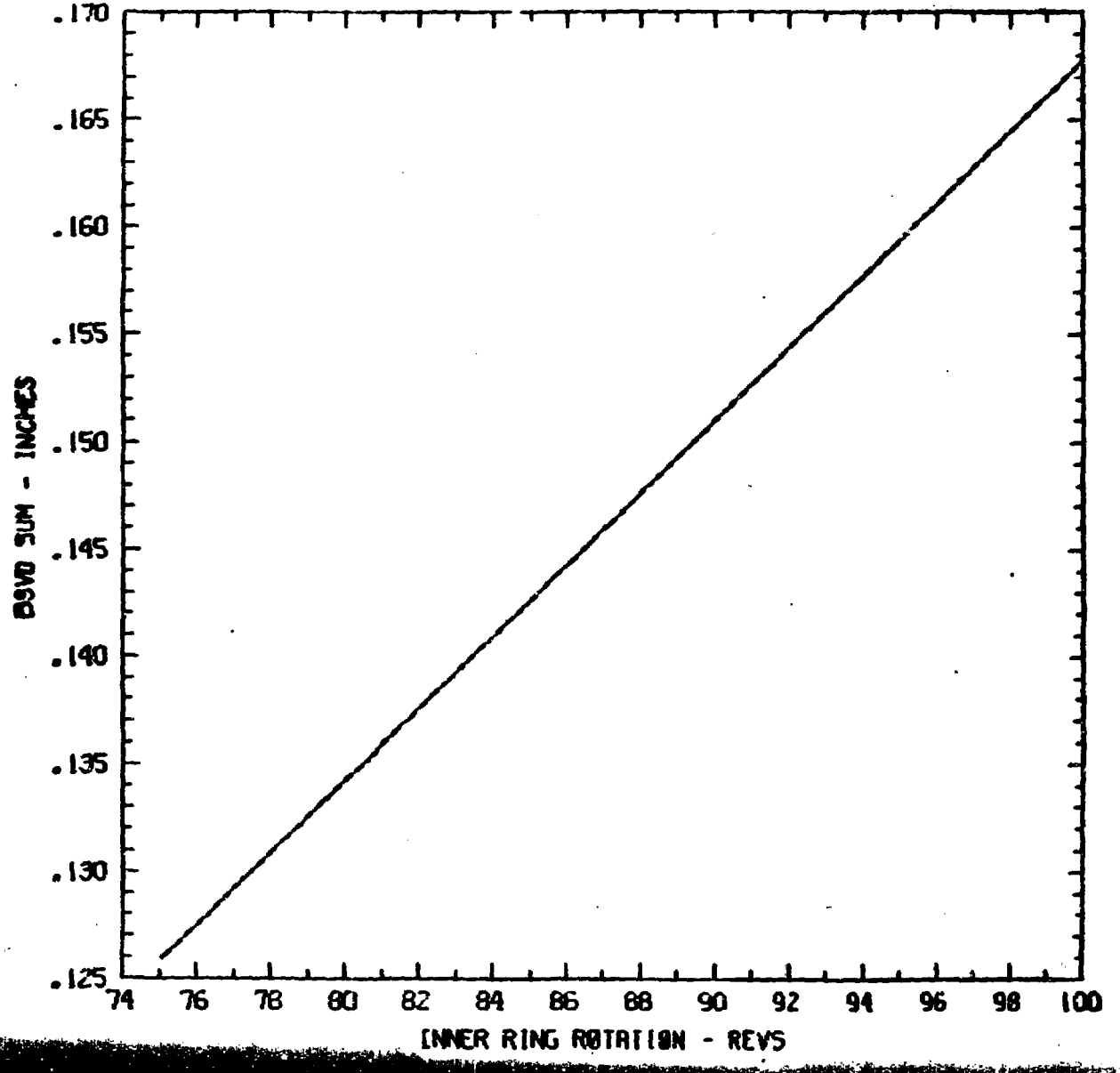

Figure 4-6 BSVD SUM (FACTØRS 2+3+4)

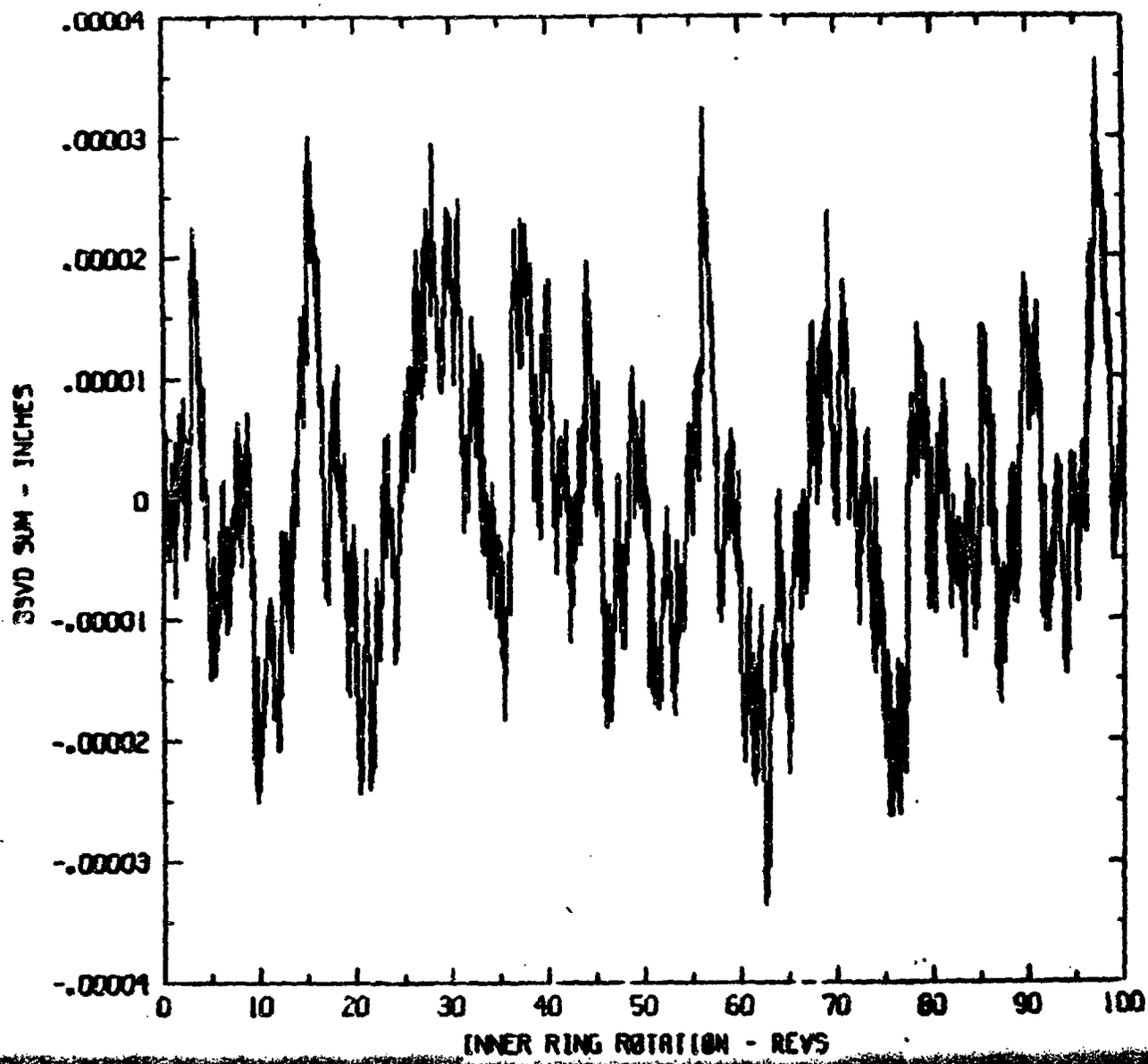

Figure 4-7 BSVD SUM (FACTØRS 2+3+4)

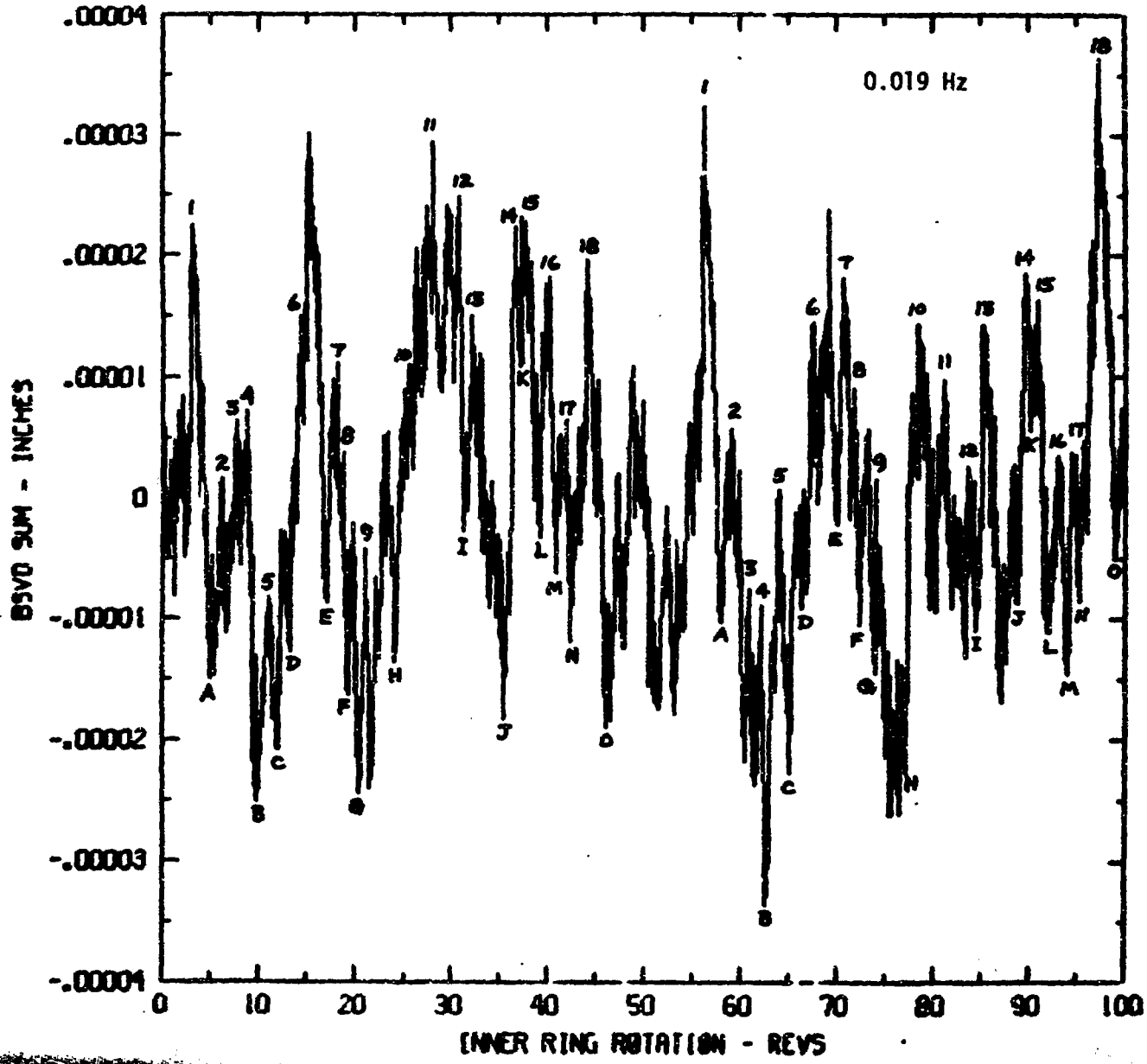

Figure 4-8 BSVD SUM (FACTORS 2+3+4)

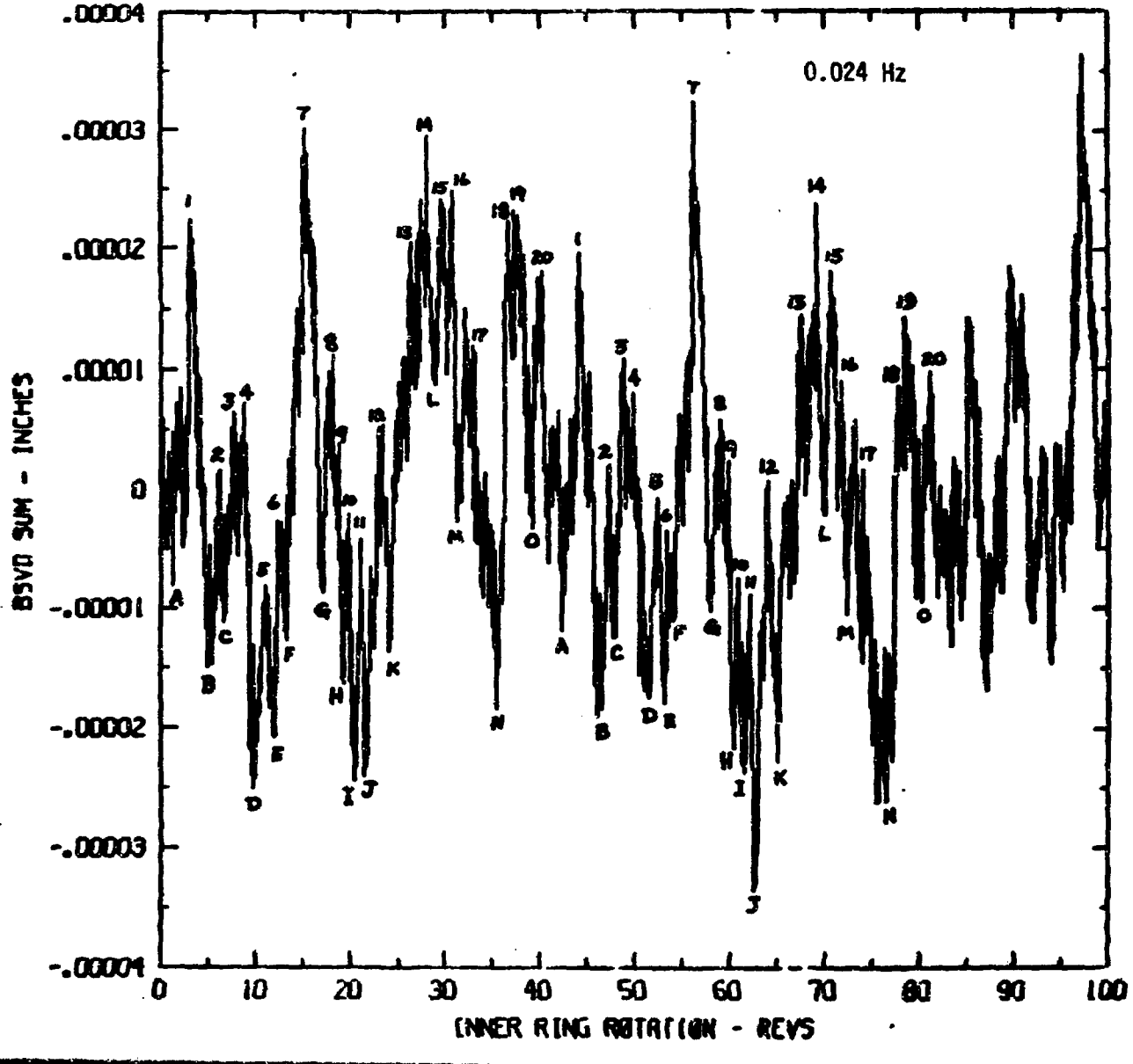

Figure 4-9 BSVD SUM (FACTØRS 2+3+4)

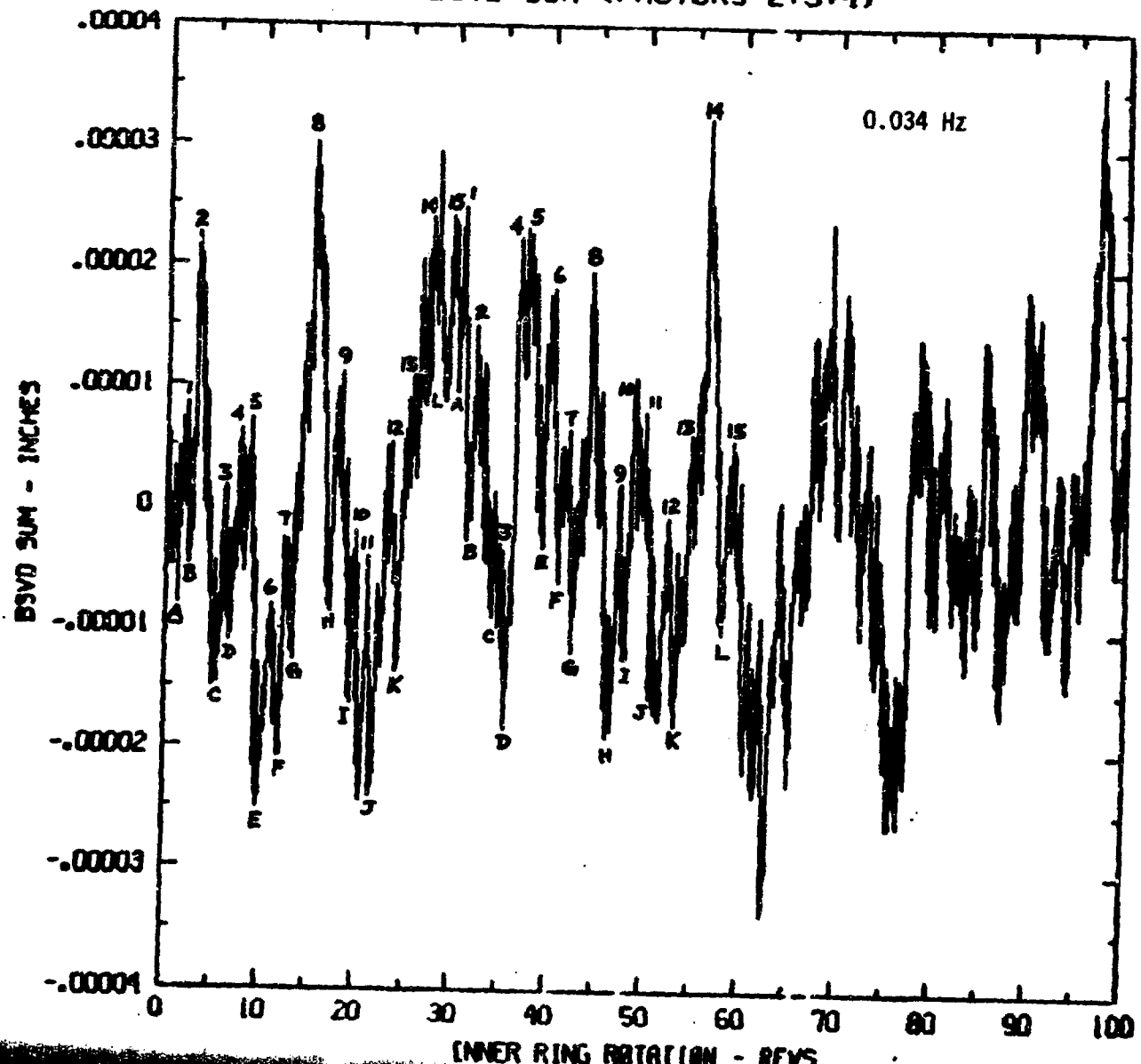

Figure 4-10 BSVD SUM (FACTORS 2+3+4)

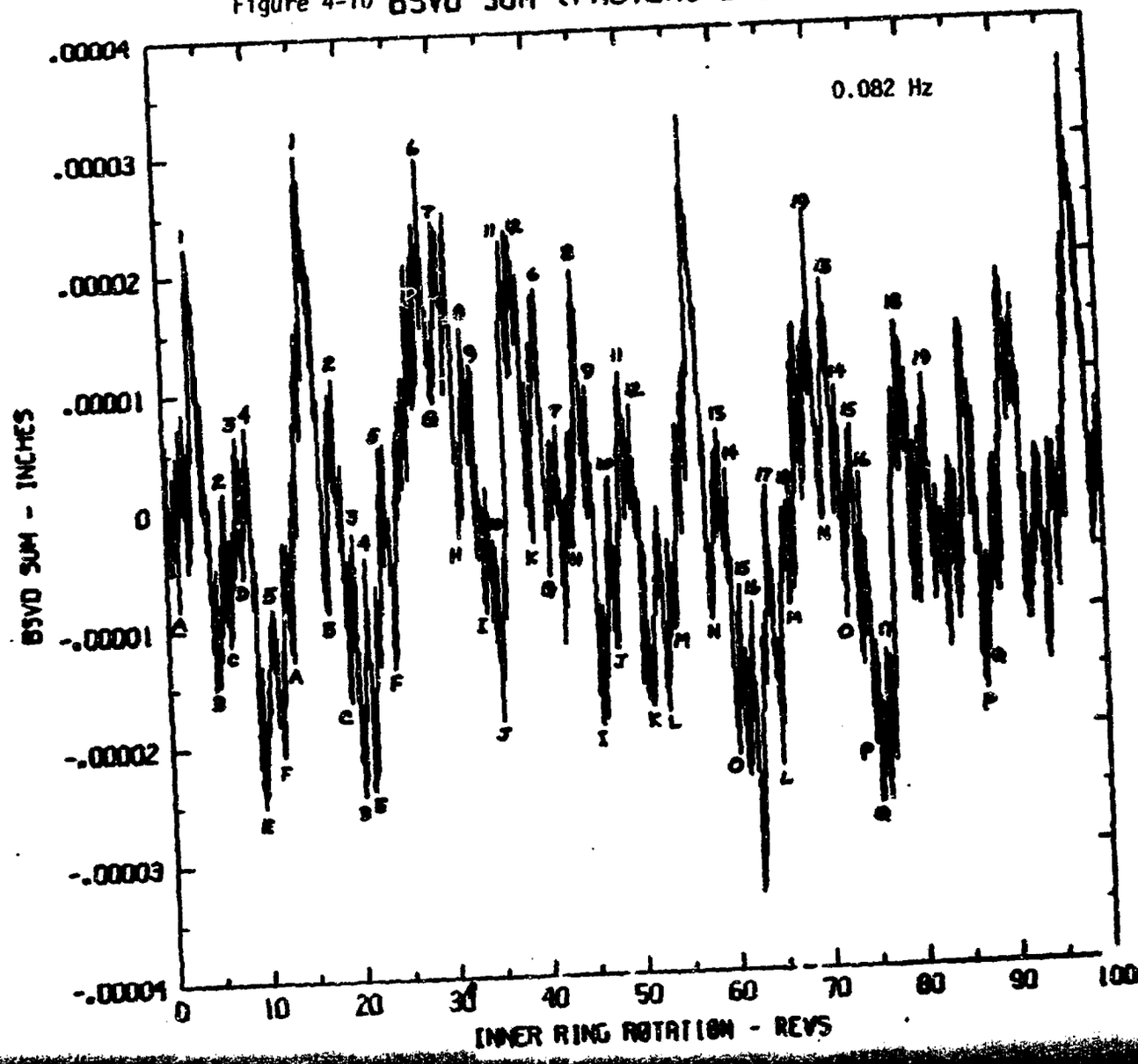

Figure 4-11 BSVD SUM (FACTØRS 2+3+4)

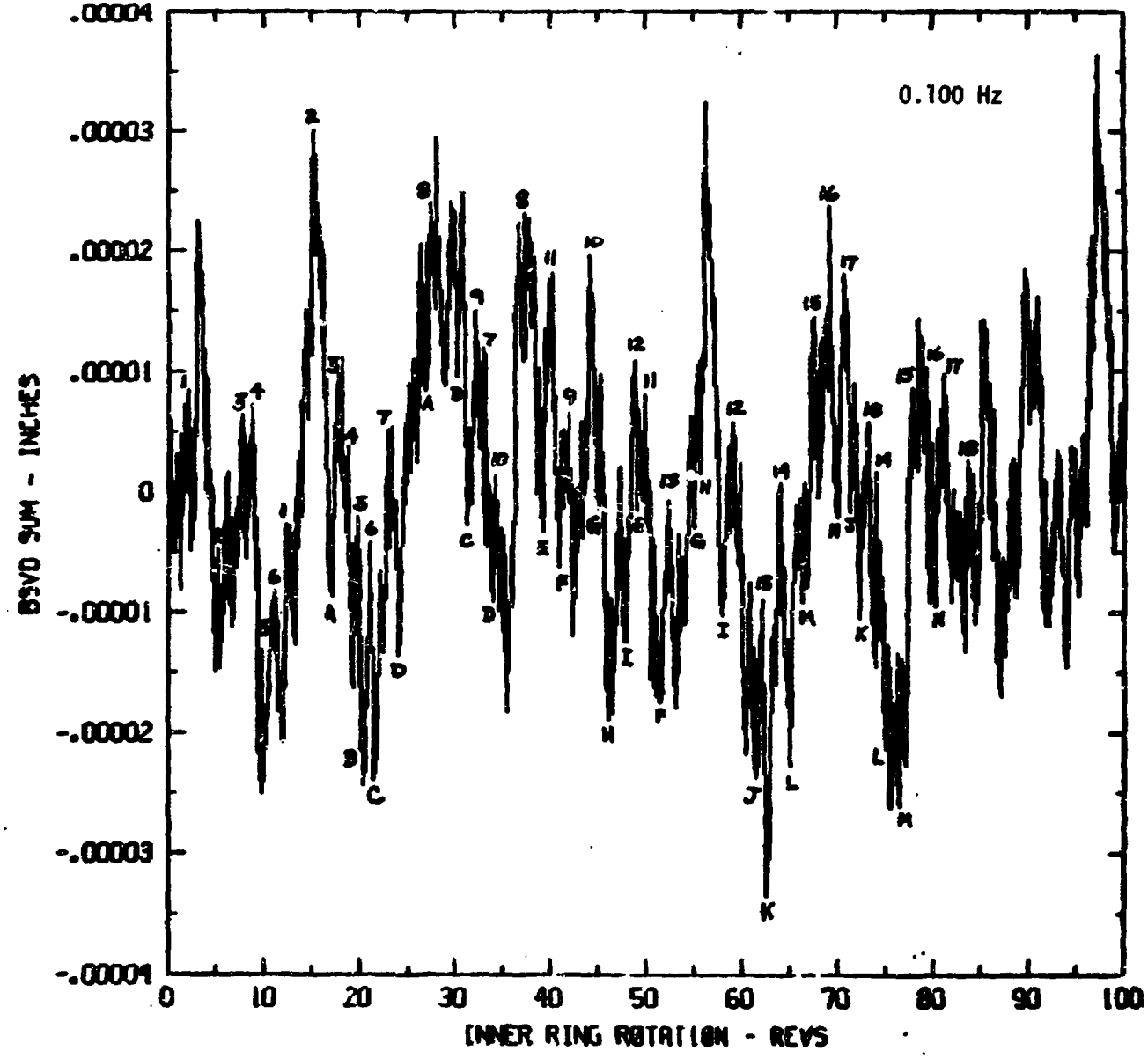

Figure 4-12 FØURIER TRANSFØRM ØF BSVD SUM

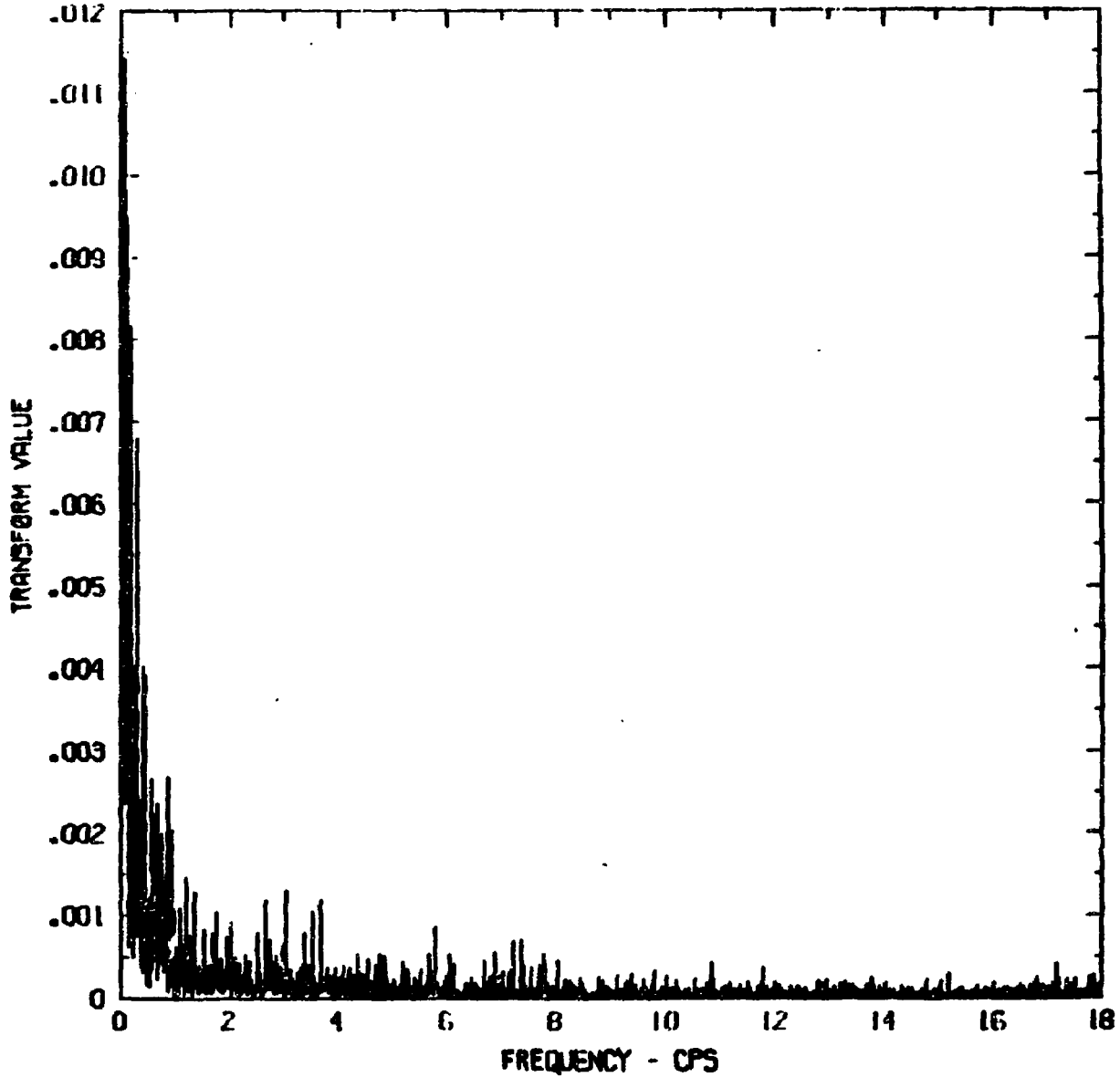

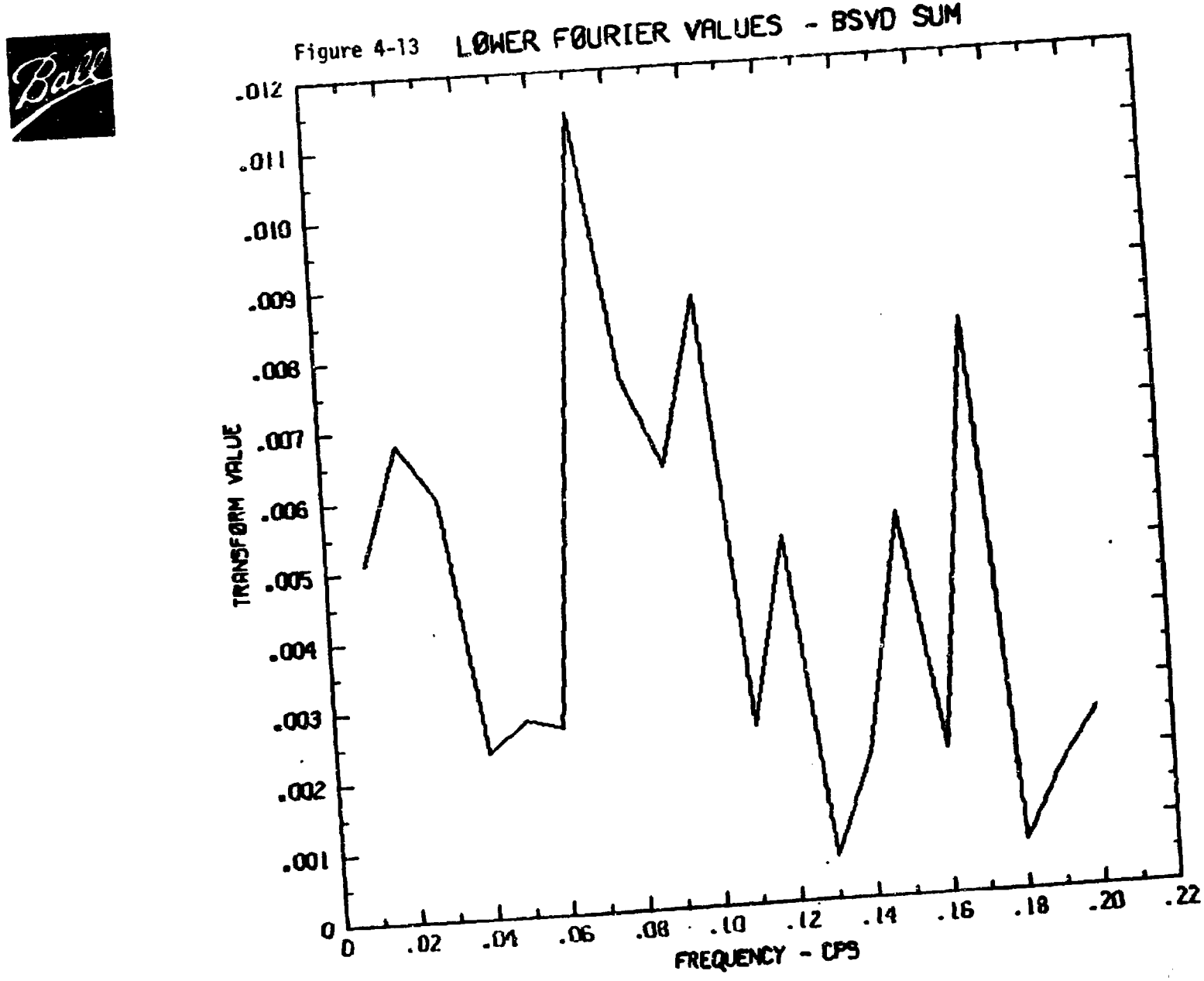
LØWER FØURIER VALUES - BSVD SUM
TRANSFØRM VALUE
.012
.011
.010
.009
.008
.007
.006
.005
.004
.003
.002
.001
0
0
.02
.04
.06
.08
.10
.12
.14
.16
.18
.20
.22
FREQUENCY - CPS

Figure 4-13

SECTION 5

CONCLUSIONS

Based upon the analyses conducted in this DMA anomaly investigation, BASD concludes that the low frequency (0.01 to 0.1 Hz) torque disturbances are caused, at least in part, by the structural bearings. In addition, these bearing torque disturbances and associated low frequencies are natural occurrences and should be expected.

As a result of the analyses of the lower bearing, we found good agreement between conditions of ball train repeat and at least one predominant torque disturbance frequency (0.019 Hz). Based upon this agreement, there is a distinct possibility that one of the torque disturbance frequencies for the upper bearing corresponds to once every 74 revolutions of the inner ring or a frequency of 0.0135 Hz.

It would be interesting to look at the low frequency torque disturbance spectrum for Flight #14 satellite to make a comparison of both normal and anomalous behavior. This comparison should be based upon the relative magnitudes of torque disturbances at specified frequencies. However, BASD does not have access to the data needed to make such a comparison.

BASD recommends that TRW review the available torque disturbance data for the frequency range 0.01 to 0.1 Hz and analyze differences between normal and anomalous system performance.

APPENDIX A

MODEL BEARING CHARACTERISTICS

Table A-1

Assumed Values for Ball Size Variation

(deviations from nominal ball diameter) in Micro-Inches

Ball No.	Ball Size Variation (μ -in)
1	0
2	2
3	-1
4	0
5	-3
6	-1
7	1
8	1
9	1
10	0
11	0
12	-1
13	-2
14	-2
15	3
16	1
17	2
18	-4
19	0
20	0
21	-1
22	4
23	0

FIGURE A-1

ASSUMED DISTRIBUTION OF BALL SIZE VARIATIONS

BEARING NO. 46265-1

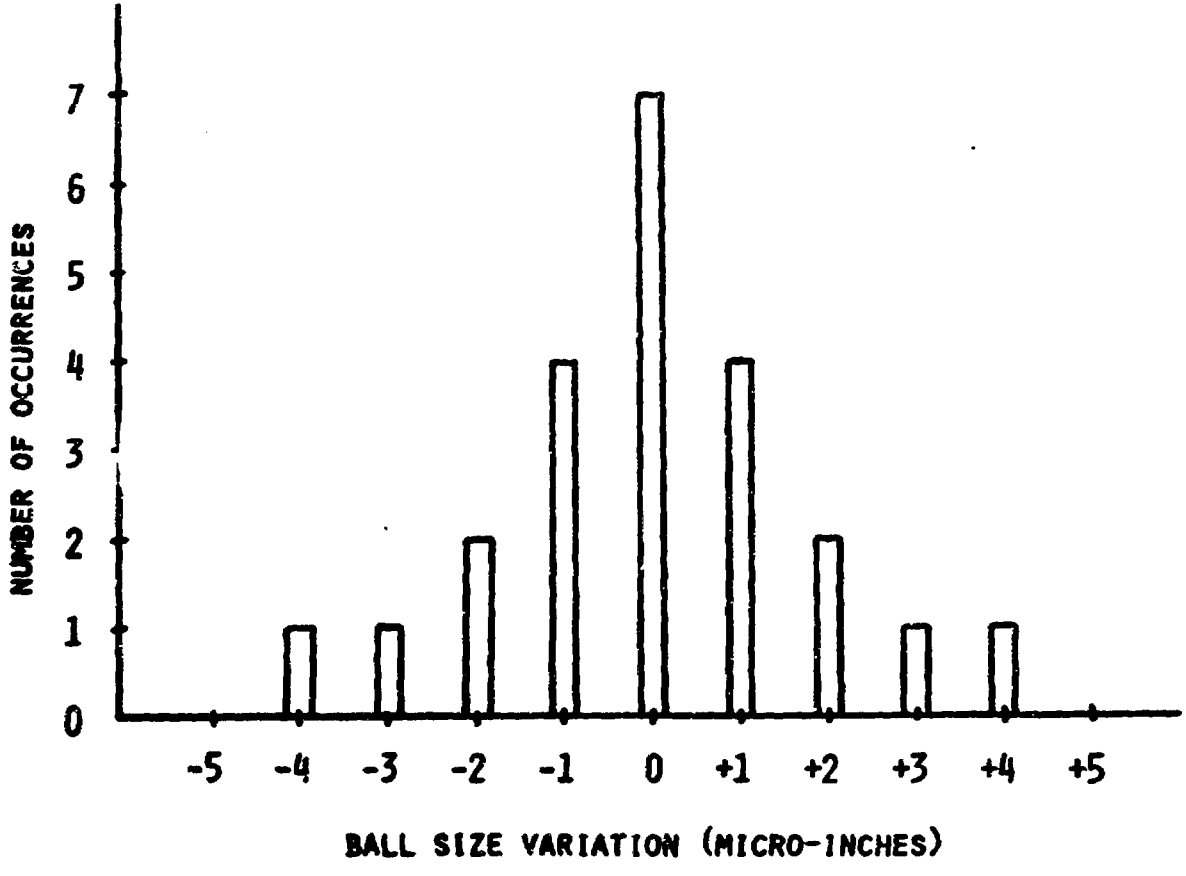

HD
2/8/82

APPENDIX B

Description of Algorithm

for Raceway Geometry Variation

Raceway Geometry Variation Algorithm

The following algorithm was used to calculate raceway deviations (half-height dimensions) for the inner and outer races.

For the inner race:

$$HI = 2 \times 10^{-6} \{H_1 \sin \Psi_i + H_2 \sin 2\Psi_i + H_3 \sin 3\Psi_i + H_4 \sin 4\Psi_i + H_5 \cos \Psi_i + H_6 \cos 2\Psi_i + H_7 \cos 3\Psi_i + H_8 \cos 4\Psi_i\}$$

For the outer race:

$$HO = 2 \times 10^{-6} \{H_1 \sin \Psi_o + H_2 \sin 2\Psi_o + H_3 \sin 3\Psi_o + H_4 \sin 4\Psi_o + H_5 \cos \Psi_o + H_6 \cos 2\Psi_o + H_7 \cos 3\Psi_o + H_8 \cos 4\Psi_o\}$$

The parameters Ψ_i and Ψ_o are defined in Section 3.5 of this report. The values used for the constant coefficients H_1 through H_8 are as follows:

H_1	= -1.171067864	H_5	= -1.880753937
H_2	= 4.129025772	H_6	= 0.2945692784
H_3	= -2.855517585	H_7	= 4.676065102
H_4	= -4.690878433	H_8	= -2.089880443

The results of using this algorithm are shown in Figure B-1 and compared with the raceway geometry profile data provided by Fafnir Bearing Company.

Figure B-1 RACEWAY IMPERFECTIONS ALGORITHM

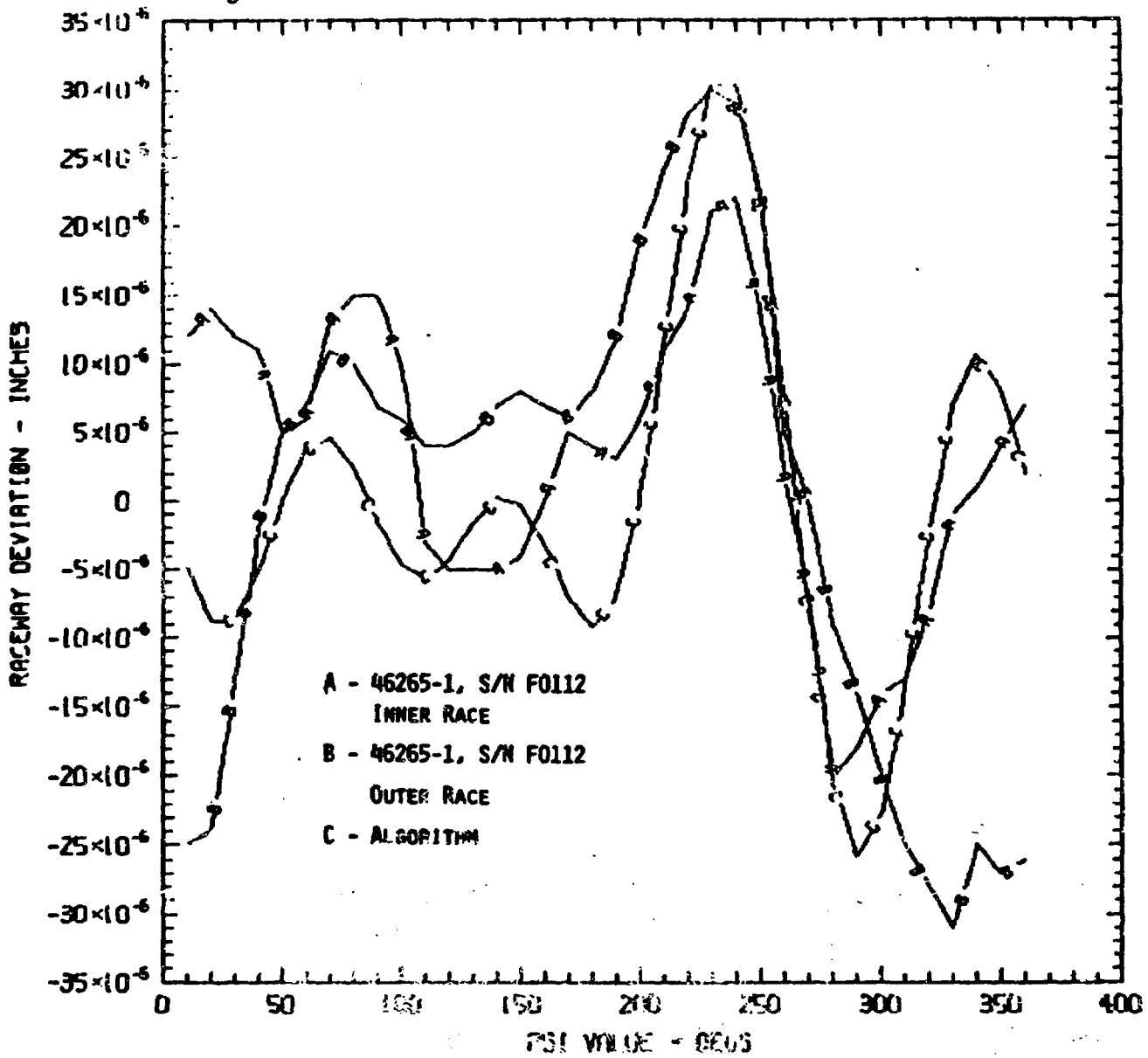

Appendix III

BEARING BEAT FREQUENCIES

Frequencies Produced by DMA (Ref: "Where are the Balls?", F. M. Manders, BASD)

As a first approximation, take the fundamental bearing frequency as that of the rotation of the retainer, ignoring effects of individual ball contact angles etc.

The retainer speed is given by equation (9) of the reference. The shaft is tilted slightly by the out of phase bearing eccentricities, and the tilt motion is defined by a beat between the motion of the two retainers. (Note in reality there is also a long period beat due to the many turns before both races and the retainer exactly line up again for each bearing.)

From (9),

$$\frac{\theta_b}{\theta_r} = \frac{1}{2} - \frac{d\cos\beta}{2E}$$

= Retainer frequency in cycles/rev. of inner shaft.

θ_b = Angle turned by retainer

θ_r = Angle turned by shaft

β = Contact angle

d = Ball diameter

E = Ball pitch circle diameter

Beat frequency between bearings = f_o

$$= \underbrace{\frac{1}{2} - \frac{d_1\cos\beta_1}{2E_1}}_{\text{Of One Retainer}} - \underbrace{\frac{1}{2} + \frac{d_2\cos\beta_2}{2E_2}}_{\text{Of Other Retainer}} = \frac{d_2\cos\beta_2}{2E_2} - \frac{d_1\cos\beta_1}{2E_1}$$

Actual dimensions of the DMA bearings are:

	Lower	Upper
Ball diameter	.5000"	.4688"
PCD	5.1400"	4.2400"
Contact angle	$14° < \beta_L < 18°$	$14.5° < \beta_u < 18.5°$

For these dimensions the fundamental beat frequency between the retainers is thus

$$f_o = 4.864 \times 10^{-2} \cos\beta_L - 5.528 \times 10^{-2} \cos\beta_u$$

For a range of possible contact angles the beat period fundamentals at a shaft speed of 1 RPS are thus:

$\beta_L{}^o$ \ $\beta_u{}^o$	10	14.5	18.5	20
$\frac{1}{f_o}$				
10	153	178	221	247 ← Spec. Limits
14	138	158	191	210
18	122	138	162	176
20	115	128	149	160

(The period is tabulated rather than the frequency as it is much easier to compare at a glance at these very low frequencies.)

Multi-Lobe Possibility

However, additional beats are introduced by imperfections in the race geometry. As an example of the effect of imperfections, consider the case of lobes in the shape of the race.

Either bearing may be 1, 2, or 3 or more lobed. Consider nine possible cases for the minimum contact angles $\beta = 14°$ and $14.5°$.

# LOWER LOBES \ # UPPER LOBES	1	2	3
1	158	*	*
2	*	79	*
3	*	*	53

(f = frequency in cycles per turn)

*High Frequency-Out of Band

$$[\text{from } f = N\,(.5 - 4.864 \times 10^{-2} \cos\beta_L) - M\,(.5 - 5.528 \times 10^{-2} \cos\beta_u)]$$

Note that the 1/1 case gives the fundamental corresponding with the corresponding β case above (underlined).

Similarly, the three low periods for 18 and 18.5° are 164, 82, 55 revs/cycle.

Thus, a real DMA with irregularities of all sorts in the races and balls if subject to slight relative tilt of the races should produce:

- A fundamental in the 130-200 turns region.
- One or more signals in the 50-80 turn region.

BASD has previously concluded that a component at about 11 revs/cycle is also to be expected.

Obviously, a more sophisticated analysis including all the factors would show other frequencies to be expected. However, the above indicates the rough order of the cyclic behavior of the tilt axis.

Comparison with Orbital Data

On 14 May 81 9444 had a pointing disturbance of just over one degree P-P. The auto correlation analysis by Aerospace shows frequency components at 55, 74, 115, and 176 revs/cycle. (By examination of the observed vs. analyzed frequencies during sinusoidal events (e.g. of 28 April 81) it can be inferred that the Aerospace analysis has some ± 6% error. Also, the PSD and Autocorrelation time scales do not match.) 9444 does not maintain constant frequency with time. Analysis of an event on 26 May for example shows frequencies of 101 and 176 R/C.

F4 similarly shows several different frequencies, though with some consistency over long periods. During an event of 30 March 78 the frequency components are about 220, 104, 31, 11 R/C. On 12 Aug 81 the components were at 157, 67, 31, 10 R/C.

The spin rate had changed from about 59 to 68 rpm during that period.

Analyses of F3 pointing are not available, but by eye similar frequencies are present.